Synthesis of CdS/CeO_2 hetero nanostructures for Photocatalytic H_2 production and simultaneous Removal of phenol and Cr(VI)

Swarnava Nandy

A Dissertation Submitted to

IIT Hyderabad

In Partial Fulfillment of the Requirements for

The Degree of Master of Science

Department of Chemistry

April, 2014

Declaration

I declare that this written submission represents my ideas in my own words, and where others' ideas or words have been included, I have adequately cited and referenced the original sources. I also declare that I have adhered to all principles of academic honesty and integrity and have not misrepresented or fabricated or falsified any idea/data/fact/source in my submission. I understand that any violation of the above will be a cause for disciplinary action by the Institute and can also evoke penal action from the sources that have thus not been properly cited, or from whom proper permission has not been taken when needed.

Swarnava Nandy

(Signature)

(– Swarnava Nandy –)

(cy12m1021)

ii

Approval Sheet

This thesis entitled "**Synthesis of CdS/CeO_2 hetero nanostructures for photocatalytic H_2 production and simultaneous removal of phenol and Cr(VI)** " by Swarnava Nandy is approved for the degree of Master of Science from IIT Hyderabad.

-Name and affiliation-
Examiner

(M. DEEPA)
-Name and affiliation-
Examiner

-Name and affiliation-
Adviser

-Name and affiliation-
Chairman

iii

Acknowledgements

I am greatly indebted to Dr. Ch. Subrahmanyam, my research supervisor for his inspiring guidance & constant encouragement throughout the course of the present investigations.

It has been great privilege & honour to be associated with him. I am very grateful to Ms. Dayamani for her support throughout the project work.

I sincerely thank:

- A. Dayamani, Krishnamurthy, P. Manoj Kumar Reddy, Sk. Mahammadunnisa for their constant support & helpful suggestion.
- Department of Chemistry, Indian Institute of Technology Hyderabad for providing basic infrastructure & extending all necessary facilities.
- All faculty members of the department, for their timely assistance whenever it was required & for their encouragement.
- All my lab mates & friends for their constant company.

Dedicated to my beloved parents

Abstract

Harvesting visible light of the solar spectrum by coupled semiconductor based systems where sensitization of a wide band gap semiconductor with a small band gap semiconductor advantageous for photocatalytic as well as photovoltaic applications. A facile one pot synthesis of several CdS/CeO_2 hetero nanostructures has been carried out without using expensive surfactants, capping agents and molecular linkers. Various techniques such as X-ray diffraction (XRD), Transmission electron microscopy (TEM), X-ray photoelectron spectroscopy (XPS), diffuse reflectance UV-Vis spectroscopy, Raman spectroscopy and BET surface area were used to characterize the samples. XRD and Raman spectroscopic data provided the information about the presence of both CdS and CeO_2 phases. TEM proves the proper dispersion and well connectivity between the CdS and CeO_2 which may be due to the single step synthesis of the composites. XPS gives the information about the presence of elements such as Cd, Ce, O, S, C and N, where the presence of latter two elements can be attributed to the in-situ C and N doping during the combustion synthesis. UV-visible spectroscopy reveals the absorption in both UV and visible regions due to the presence of both CeO_2 and CdS. The visible light activity of the composites have been ascribed by the H_2 production from water by using sacrificial reagents, simultaneous removal of phenol and Cr(VI) from aqueous streams. Among the synthesized composites CdS/CeO_2 (1:1) has shown superior activity which can be attributed to the optimum sensitization of CeO_2 which induces enhanced electron transfer from CdS to CeO_2 that decreases the exciton recombination.

Nomenclature

XRD: X-ray diffraction

UV-Vis Spectroscopy: Ultra Violet- Visible Spectroscopy

XPS: X-ray Photoelectron Spectroscopy

TEM: Transmission Electron Microscopy

GC: Gas Chromatography

Contents

Chapter 1

Introduction

1.1 Search for Clean and Renewable Energy Source

Energy and environmental issues are important topics at global level in the present day scenario [1-3]. It is indispensable to generate clean energy sources in order to solve these issues. Hydrogen plays an important role as an energy carrier because it is the ultimate clean energy source and it can be used in applications such as fuel cells and chemical industries [4-6]. At present, hydrogen is mainly produced from fossil fuels such as natural gas by steam methane reforming as represented by the following equations [7].

$$CH_4 + H_2O \longrightarrow CO + 3H_2 \quad \ldots\ldots\ldots\ldots\ldots\ldots\ldots\ldots\ldots\ldots (1)$$

$$CO + H_2O \longrightarrow CO_2 + H_2 \quad \ldots\ldots\ldots\ldots\ldots\ldots\ldots\ldots\ldots\ldots (2)$$

In this process fossil fuels are consumed and CO_2 is emitted. Gradual lack of fossil fuel has become a major problem since they are obtained from the nature in the form of oil, natural gas, coal etc. Moreover as they are obtained from the nature the supply is not enough with respect to the demand of the society. Also fossil fuels are depleting rapidly and cause harm to the society by causing acid rain, ozone layer depletion, air pollution, oxygen depletion and climate change etc [8-9]. It indicates that there is an immediate need for a clean energy source which causes no virulent

effect to the society and should have enough supply of energy from that source so that it can satisfy the requirements.

Although H_2 can play an important role as an energy carrier about 95% H_2 is still derived from fossil fuels and obtained by steam reforming or catalytic decomposition processes. Among these varieties only H_2 has attracted much attention because of its distinct properties [10-12].

- Low Gibbs free energy of formation, no toxicity, lightest element.
- It has highest mass specific energy. For example: 119.3 MJ/Kg for H_2 compared to 44.5 MJ/Kg for gasoline makes it favorable fuel of choice.
- Ecologically neutral ideal candidate to serve as fuel cell, produce little emissions.
- It is safer than other commonly used natural gas either methane or petrol vapour (due to high diffusion co-efficient).
- The major advantage is that it can be produced from water which is the most easily available source of hydrogen.

Therefore Hydrogen can be considered as the simplest possible closed-shell molecule that can attain great scientific and technological interest as a primary energy carrier and as a potential transportation fuel [13]. However the present steam methane reforming used for the H_2 production from hydrocarbons is non-renewable [13-16]. Therefore, there is a need to search for other methods to produce hydrogen from renewable energy sources. The solar energy that falls on the earth's surface far exceeds our energy consumption, and is the only renewable energy that has the capacity to fulfill current energy demand or those predicted for the future [18]. The production of hydrogen by using water, catalyst and solar energy is an ideal future

energy source, independent of fossil reserves. For the economical use of water and solar energy catalyst that are sufficiently stable, inexpensive and capable of harvesting light are required. That's why it requires some special reagents that have this property to do so. Photocatalysts are one of these reagents that are capable to act in this way. Therefore photocatalyst can play crucial role to provide clean energy to the society. Direct splitting of water using a particulate photocatalyst would be a good way to produce clean and recyclable hydrogen in a large scale. As a result of these potential environmental and economic benefits, photocatalytic hydrogen production has been receiving increased attention [19]. Photocatalytic water splitting promises to enable sustainable large scale hydrogen based energy system using solar light, and great attention has been paid for the development of photocatalysts. It is necessary to develop photocatalysts that function under visible light to utilize sunlight efficiently. For the last 30 years there are various functional photocatalysts found that can function under visible light.

1.2. Water pollution and photocatalysis

Water pollution has become one of the onerous matters to take challenge against it. It occurs when surface water or ground water discharged with contaminants has lost its utility to use for the human life [20]. When the components of water bears with increasing concentration of many elements such as Ca, Be, Mg etc it is said to be polluted. Water pollution is the contamination of water bodies (e.g. lakes, rivers, oceans, aquifers and groundwater) with many organic and inorganic matters. Generally water pollution occurs when the pollutants are directly or indirectly discharged into water bodies without adequate treatment to remove noxious compounds [21-23]. Water pollution affects plants and organisms living in these bodies of water. In almost all cases the effect is damaging not only to individual species and populations, but also to the natural biological communities. Water

pollution is a major global problem which requires ongoing evaluation and revision of water resource policy at all levels [24-26].

1.2.1. Water Treatment Techniques

The treatment of contaminated water mainly involves the techniques such as mechanical, biological, physical, and chemical processes. After filtration and elimination of particles in suspension which are called as primary treatments, biological treatment is used to perform as a secondary treatment. [27-30]. Unfortunately, there are certain pollutants which are said to be bio-recalcitrant (non-biodegradable), for which much more effective non-reactive systems, such as air stripping, adsorption on granulated activated carbon, incineration, ozone and oxidation (tertiary treatments), are needed. These processes are mainly to treat the wastewaters, and therefore to improve water quality, but some of these technologies (such as adsorption and filtration) only concentrate the pollutants by transferring them to other phases. Therefore the next problem may be how to properly dispose the new pollutant rich streams. Generally organic pollutants are not completely removable by traditional water treatment technologies like distillation, reverse osmosis, ion-exchange, carbon adsorption, micro porous membrane filtration. On the other hand distillation and reverse osmosis remove a wide range of water contaminants but one of their major disadvantages is that they also remove the good stuff - that is, the trace mineral elements (heavy metals e.g. copper, zinc, iron) that are also present in water and vital to human health [31]. Therefore, management of toxic chemicals with strict environmental legislation drives the development of clean and green processes, to eliminate the pollutants before they are disposed into the environment. Furthermore, for these processes to be effective, complete mineralization and degradation of all organic and inorganic contaminants from water and wastewater, are required.

1.2.2. Advanced Oxidation Processes

The strong potential of tertiary treatments called Advanced Oxidation Processes (AOPs) for bio-recalcitrant wastewater treatment is universally recognized today, and many researchers around the world are devoting their efforts to the development of these processes [32-35]. Although they make use of different reaction systems, AOPs are all characterized by the same chemical feature: the production of hydroxyl radicals ($OH^{\bullet}$). These radicals can virtually destroy any organic contaminant present in water. They can even destroy pollutants that are not amenable to biological treatments, which are all characterized by high chemical stability and difficulty to be completely mineralized. In order to apply a decontamination technique to these cases, it is necessary to adopt reactive systems much more effective than those adopted in conventional purification processes. Among AOPs, heterogeneous photocatalysis has confirmed its efficiency in degrading a wide range of organic contaminants into CO_2 and water. Over the past few decades, photocatalysis has been the subject of extensive research in the removal of contaminants in air and water streams. Several features, such as ambient operating conditions, complete destruction of parent and their intermediate compounds and relatively low operating cost have confirmed its applicability to water treatment.

1.2.3. What is Photocatalysis…?

Photocatalysis is generally a combination of photochemistry and catalysis. This implies that both light and a catalyst are needed to enhance the rates of thermodynamically favorable ($\Delta G < 0$) but kinetically slow photophysical and photochemical transformations. Photocatalysis has the capability of performing both oxidation and reduction which is a unique property of it compared to other reactions where either oxidation or reduction may takes place. Simply photocatalysis can be defined as “a catalytic reaction involving light absorption by a catalyst or a substrate”[36].

Photocatalysis is believed to mimic natural process photosynthesis which involves the conversion of CO_2 and H_2O into starch (chemical energy) in the presence of sunlight

whereas photocatalysis involves the destruction of toxic organic compounds into CO_2 and H_2O.

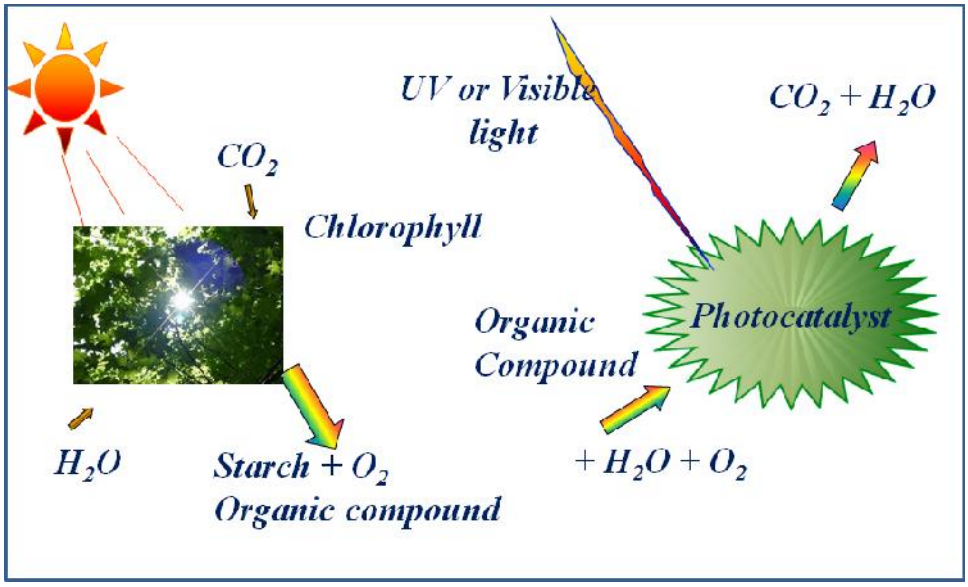

Figure 1.1. Diagrammatic representation of similarity between photosynthesis and photocatalysis

1.2.4. Mechanism of photocatalysis

TiO_2 under suitable irradiation (energy greater than band gap) can undergo excitation to produce electron hole pairs. As shown in figure II the produced hole can combine with OH^- from the water to form $OH^{\cdot}$, which is a strong oxidizing agent next to fluorine. On the other hand the electron present in the conduction band of TiO_2 may react with O_2 from atmosphere or O_2 dissolved in water to from peroxide radical which on further reactions can produce again $OH^{\cdot}$ which is responsible for the oxidation capability of a photocatalyst.

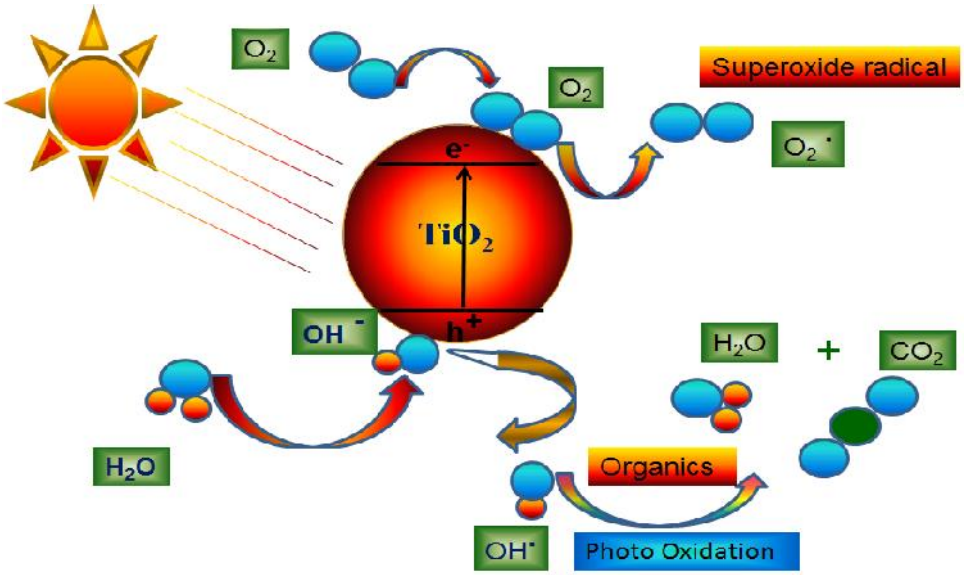

Figure 1.2. Diagrammatic representation of photocatalytic mechanism

1.2.5. Recombination of excitons

Since the excitons produced during the irradiation of TiO_2 are not stable they can recombine in several ways such as surface recombination and volume recombination. If the electron and hole recombines just before reaching the surface it is termed as surface recombination whereas the recombination taking place within the bulk of the material is called as volume recombination. Volume recombination can be minimized by preparing the material in nano size, so that the time taken for the electron to reach the surface might be less. Surface recombination can be reduced by doping of TiO_2 where the dopant can trap the electron thereby preventing the exciton recombination. Figure 1.3. clearly depicts the different types of recombination that are taking place in a photo catalytic process.

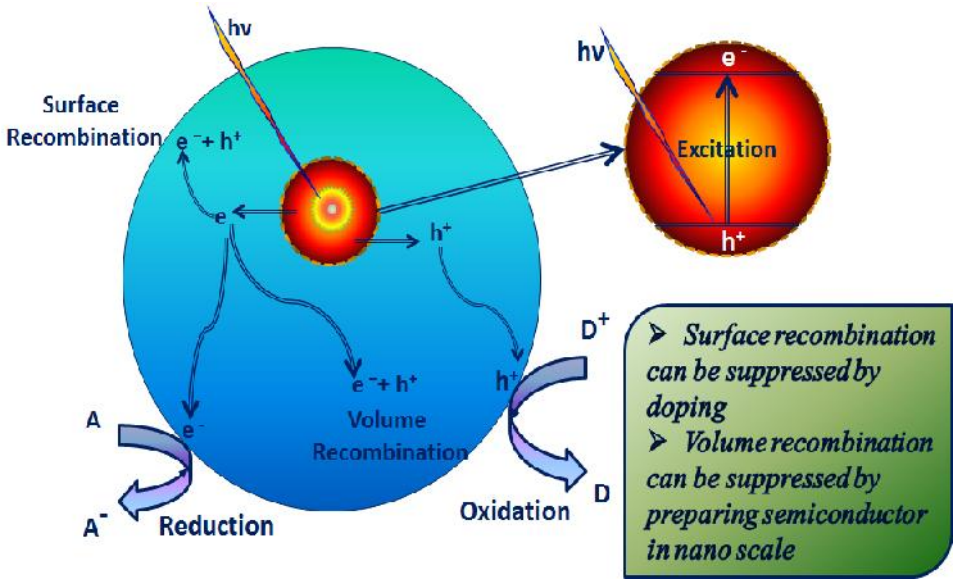

Figure 1.3. Diagrammatic representation of different recombination processes taking place in photocatalysis

1.2.6. Need for a visible light active photocatalyst

Since the discovery of photocatalytic splitting of water on titania electrodes by Fujishima and Honda in 1972 [37] heterogeneous photocatalysis have gained much importance. Afterwards tremendous research has been done in understanding the fundamental processes and in enhancing the photocatalytic efficiency of TiO_2 which are often related to energy renewal and energy storage [38-42]. Many semiconductors have been tested so far as photocatalysts, although only TiO_2 in the anatase form seems to have the most interesting required attributes; such as high stability, good performance and low cost. In this respect, the photodecomposition power of TiO_2, for a wide variety of organic compounds present in water, has been reported in the literature. However, its wide band gap energy (3.0 eV for rutile and 3.2 eV for anatase) means that only 4% of solar spectrum could be used as light source in an industrial application. Therefore, to use visible sunlight, which composes the largest part of solar radiation, a photocatalyst TiO_2 with strong absorption in the visible region should be developed.

1.3. Methods for Preparing Visible Active Titania

Due to the relatively large band gap of TiO_2 (3.2 eV), UV light must be used in its photo excitation process, allowing with this the use of only 5% of the solar light that reaches the surface of the earth each day. Because of this, a great deal of research has focused on lowering the threshold energy for the photo excitation process. As a consequence, a larger fraction of the solar spectrum could be used effectively for photocatalysis and other processes. Thus, the development of a photocatalytic TiO_2 system capable of using natural sunlight to degrade organic and inorganic contaminants in wastewater can be achieved. These improvements in the overall performance of titania have been led by two main lines of research: dye sensitization or coupling with small band gap semiconductor and doping [43].

1.3.1. Dye sensitization

Dyes are natural light absorbers and electron transfer agents. They have been used for energy conversion in a process that copies the plant photosynthesis mechanism in electrochemical energy converting solar cells [44]. Dye sensitization is a process occurring when a light-excited dye molecule adsorbed at the semiconductor surface injects electrons into the conduction band of the semiconductor substrate. Titania based dye sensitization has potentially low cost, low environmental impact, and good power conversion efficiency. Figure 1.4. clearly shows the electron transfer processes taking place in case of dye sensitized TiO_2 photocatalyst. However, its more general use is limited by low quantum efficiency, high carrier recombination, low adsorption of the dye to the surface of the semiconductor material, dye desorption from the TiO_2 due to solvent effects, lack of long-term stability of the dye under light and heat, etc [45, 46].

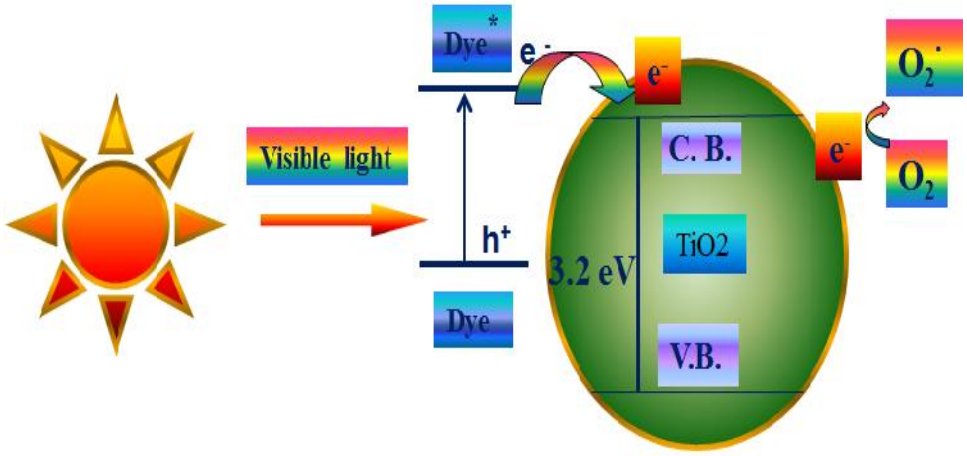

Figure 1.4. Diagrammatic representation of photocatalytic mechanism in dye sensitized TiO_2 system

1.3.2. Coupling with small band gap semiconductor

Sensitizing TiO_2 with a small band gap semiconductor like CdS, CdSe, PbS, SnS_2, SnS, Bi_2S_3, In_2S_3, $CuInS_2$, etc. is gaining increasing interest because of their matching conduction band levels that can prevent recombination of hole and photoelectron [47−59]. Moreover these hybrid photocatalysts may have the potential to mimic the natural photosynthesis [60]. CdS is one of the most suitable metal chalcogenides for photocatalytic H_2 production due to its high activity under visible light and sufficiently negative flat-band potential [61,62]. Such coupled semiconductor hetero structures (or nano composites) can also offer the advantages like synergetic effect, efficient charge separation and migration, expanded visible light response, and improved photostability over the individual components. TiO_2 plays dual roles in the hybrid system as it stabilizes by preventing the aggregation of CdS and also enhances the charge separation by forming a potential gradient at the interface of CdS and TiO_2. It has been reported that the rate of photo induced electron transfer at CdS increases by tenfold in the presence of TiO_2, and thereby photocatalytic efficiency [63-65]. Figure 1.5 represents the schematic of photocatalytic mechanism in coupled semiconductor systems.

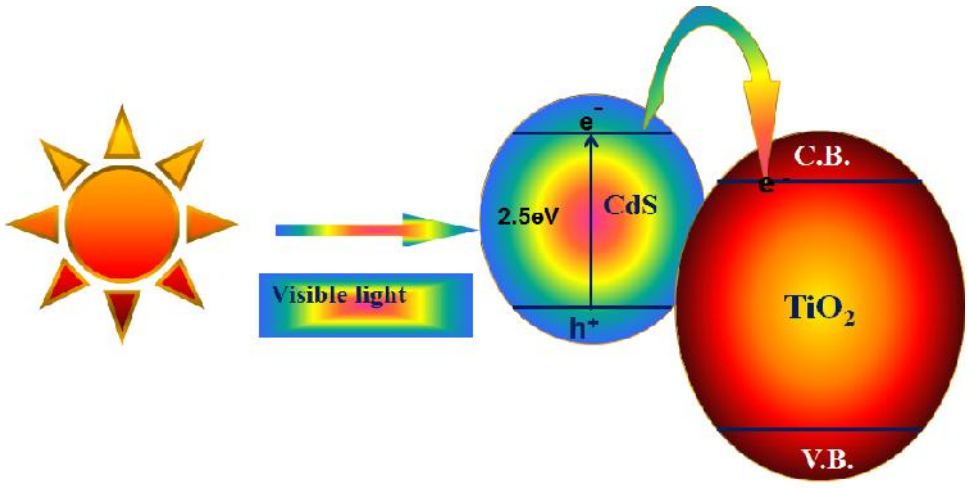

Figure 1.5. Diagrammatic representation of photocatalytic mechanism in coupled semiconductor system

1.3.3. Doping

There has been a significant interest recently on both non-metal and transition metal doping of titanium dioxide TiO_2. The use of the so-called impurities creates extrinsic properties in the oxide host and a decrease in the band gap energy. The consequence is an increase in photoactivity under visible light irradiation. Different types of doping are reported for titania [66, 67], such as doping of nitrogen, carbon, sulfur and metal ions.

1.3.4. Nitrogen doping

The idea of doping of titanium dioxide materials with nitrogen and other anionic species was presented in 2001 [68]. This report shows theoretical results for the substitution of C, N, F, P, or S atoms for oxygen atoms in the titania lattice. The study of density of states (DOS) for anatase TiO_2, suggests that substitutional doping using nitrogen is more effective due to the mixing of nitrogen 2p states with oxygen 2p states, thus causing a significant decrease in the width of the overall band gap [68]. The theoretical predictions

presented in the report were supported by experimental results using visible light and photooxidation tests for nitrogen doped TiO_2.

1.3.5. Carbon doping

Among the various approaches to improve TiO_2 visible light activity [68,69], doping by anions has been extensively studied as the most prominent approach for the development of visible light activated photocatalysts with carbon being the most favorable dopant. It is reported that carbon doping not only can improve the significant adsorption of organic pollutant molecules on the catalyst surface [70,71], but also can enhance the conductivity of TiO_2, which can thereby facilitate the charge transfer from the bulk of the TiO_2 to the surface where the desired redox reactions takes place [72,73]. Moreover theoretical studies also claimed that carbon doping has a potential advantage over nitrogen doping [74].

1.3.6. Sulfur doping

Substitutional doping of sulfur similar to that of nitrogen doping has been reported [68]. However, sulfur doping was dismissed experimentally due to its large ionic size [68].The idea was that substitution of sulfur at the oxygen sites could significantly modify the electronic structure of TiO_2, but conventional doping techniques could not achieve this because sulfur has a larger ionic radius compared to N or F [68]. Furthermore, narrowing effect and delocalization of the valence band edge is expected to occur only in the case of higher sulfur doping levels [75].

1.3.7. Doping with transition metals

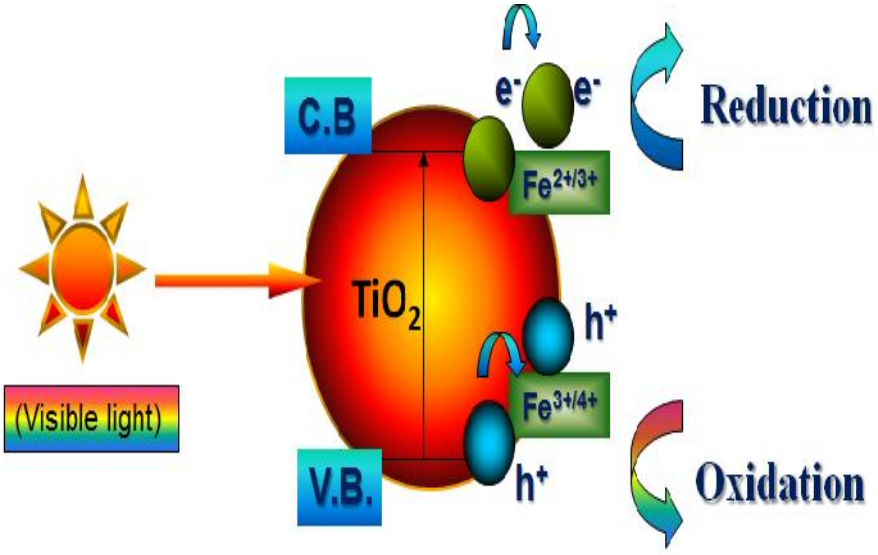

Figure 1.6. Schematic representation of photocatalytic mechanism in metal doped TiO_2

Although the effect of metal doping of TiO_2 has been studied widely in order to improve its catalytic activity, ambiguous conclusions are still often found. Some authors postulated that doping with cations having a valence higher than +4 can increase the photoactivity [76] while doping with trivalent metal ions would show a negative effect in photocatalytic activity [77].

However, both positive and negative effects have been reported for the photocatalytic activity of metal doped TiO_2. For example, doping using Fe^{3+}, Mo^{5+}, Ru^{3+}, Os^{3+}, Re^{5+}, V^{4+}, and Rh^{3+} was claimed to increase the photoreactivity for oxidation and reduction processes however, the same study reported the opposite effect with Co^{3+} and Al^{3+} showing a decrease in photoreactivity [78]. Similar effects were found with low valence (Fe^{3+};Co^{2+};Ni^{2+}) and high valence cations (Mo^{5+}, Nb^{5+}, W^{6+}) [79]. Theoretically, the addition of Ti^{3+},V^{3+}, Cr^{3+}, Mn^{3+}, and Fe^{3+} in both anatase and rutile TiO_2 crystal modifications were studied and it was concluded that there is a significant band gap narrowing effect for anatase; whereas, for the rutile modification no effect is expected [80].The positive effect of

metal doping is believed to be related to the energy level and d-electron configuration of the dopants in the host structure [78].

Additionally, it is believed that the presence of metal species allows the formation of a permanent space charge region on the surface of the semiconductor, improving the separation of photocarriers. Other authors conclude that although metal ion doping should decrease the photo threshold energy of TiO_2, the metal ion may also serve as a recombination center for electrons and holes, thus diminishing the overall activity of the photocatalyst [79, 81]. In conclusion, at present there is still no consensus in this matter and more research is needed in order to resolve the conflicting metal doping effects reported [81]. Figure 1.6. shows the schematic representation of photocatalytic mechanism in metal doped TiO_2.

1.3.8. Synthetic methods for preparation of TiO_2

While different methods have been used for the preparation of ceramic oxides and inorganic materials in general, most commonly solid-state synthetic routes are used. However, these routes are time consuming and have high energy requirements [79]. Thus a search for more energy efficient methods in the preparation and improvement of oxide materials is relevant. A large number of methods is emerging as synthetic routes for the preparation and doping of titania. These include: electrochemical methods [82, 83], ionized cluster beam deposition [84], aerosol process [85, 86], gas condensation [87], homogeneous precipitation at low temperatures [HPPLT][88], sol-gel process [89], mechanochemical synthesis [90],hydrothermal process [91-93] and combustion synthesis [79, 94-97]. Comparatively, each method has advantages and disadvantages. For instance, aerosol process gives a pure product with no multiple steps, but the high temperature required leads to aggregation of particles. Among low temperature methods, the hydrothermal approach is attractive because of the use of $TiOSO_4$ as raw material and the use of a low temperature (300^o C) in aqueous media. However, the total time required varies between 1-6 hours and

post preparation annealing of samples is required (temperatures higher than 450 o C). Sol-gel process is also a low temperature method, but it incorporates a series of successive steps and costly chemicals and does not easily allow for control of composition. In addition, the sample must be annealed in order to improve the photocatalytic activity [89]. On the other hand, combustion synthesis exhibits advantages over the other methods for the preparation of TiO_2. Thus the present work has utilized this synthetic technique for the synthesis of C-doped TiO_2 nanomaterials.

1.4. Combustion Synthesis

Combustion synthesis, also known as self-propagating high-temperature synthesis (SHS), uses a highly exothermic redox chemical reaction between metals and nonmetals, for the synthesis of oxide and non-oxide materials [79]. This method presents a variety of advantages that include: low energy requirement, generation of high-reaction temperature, short duration of reaction, high yields, highly crystalline products, simplicity and low cost [94, 98]. The synthesis is obtained through an exothermic, rapid, self-sustaining and self-propagating reaction. This is possible due to the large amount of heat released by the reaction itself, and is this exothermicity what makes the technique special and attractive [93, 98]. As with any other combustion reaction, combustion synthesis requires the presence of an oxidizer (oxygen or any other electronegative element) and a fuel (source of reducing elements to the reaction).

1.4.1. Synthesis of coupled semiconductors

Various preparation strategies, such as precipitation, micro emulsion process, chemical bath deposition (CBD), chemical vapor deposition, and electrochemical deposition, have been studied to synthesize CdS/metal oxide nano composites [99-103]. Many of these techniques deal separately the preparation of metal oxide nanostructures and sensitization with low band gap semiconductor. It is well known that the contact ability between QDs and metal oxide is less strong when compared with metal and metal oxide.

Hence synthesis of stable and active and QDs/metal oxide composite materials is still a challenge [104].

Over the past few years, intensive research has been focused on transition metal oxides such as ZnO, TiO_2, Fe_2O_3, etc [105–107]. However, little attention has been paid to rare earth oxides, which have been widely used in up conversion materials, high-quality phosphors, time-resolved fluorescence labels for biological detection, catalysts, and catalyst supports due to their outstanding optical and catalytic properties [108–112]. Recently, the optical, catalytic and electrical properties of CdS doped with rare earth elements have been studied [113–115] but investigations of CdS/rare earth oxides hetero structures are still rarely reported. Thus it is highly desirable to investigate the properties of CdS/rare earth oxide hetero structures, especially for their photocatalytic activity. To evaluate this issue, we examined a combination of CeO_2 and CdS for photocatalytic hydrogen generation because CeO_2 has a suitable band gap (3.2 eV). Moreover, CeO_2 has been recently used as a photoactive material in solar cells and a photocatalyst in the degradation of dye pollutants and hydrogen evolution [116–120]. In addition to this CeO_2 has the following advantages over TiO_2: Titanylnitrate is not readily available, for the synthesis of titanylnitrate expensive Ti(IV) iso-propoxide is needed, Handling of Ti(IV) iso-propoxide is difficult whereas Ce(IV) nitrate is readily available and can be handled easily.

Therefore in the present study a novel synthesis of CdS/CeO_2 hetero nanostructures by using combustion synthesis followed by characterization to understand the physico-chemical properties has been carried out. The catalytic activity of the as prepared catalysts were evaluated for H_2 production from water containing sacrificial agents and also for the simultaneous and individual removal of phenol and Cr(VI).

Chapter 2

Characterization Techniques

2.1. X-ray Powder Diffraction (XRD)

X-ray powder diffraction (XRPD) is an important analytical technique widely used for the characterization of crystalline materials to identify unknown substances, by comparing diffraction data with those in the international data base [121-124]. In fact each crystalline solid produces distinctive diffraction patterns. When a monochromatic X-ray beam passes through a crystalline sample, it interacts with the electrons in the atoms, resulting in scattering of the radiation. If the matter is crystalline, i.e. the atoms are organized in planes and the distances between the atoms are of the same magnitude as the X-rays wavelength, constructive and destructive interference will occur. The process of diffraction is described in terms of incident and reflected (or diffracted) rays, each forming an angle, θ, with a fixed crystal plane. In particular, when the interaction of the incident rays with the sample produces constructive interference (Fig. 2.1.), the diffraction phenomena satisfy the so-called Bragg law [125].

$$n\lambda = 2d \sin\theta \qquad (1)$$

where:

λ = incident light wavelength.

n = integer positive number (0,1,2,3, etc.).

d = interplane spacing.

θ = angle between the incident radiation and the planes (h k l).

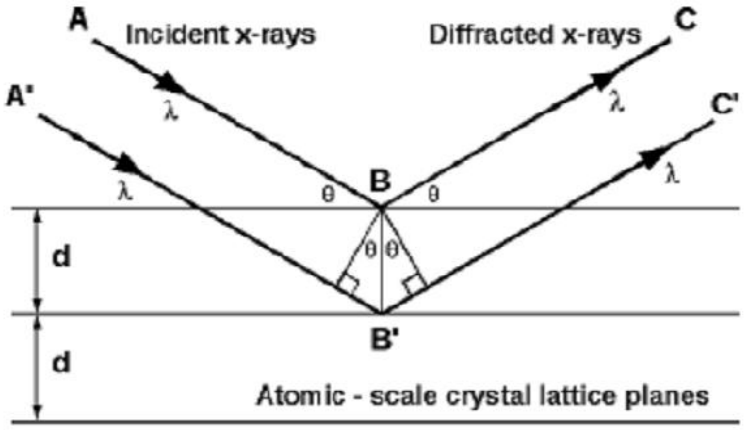

Figure 2.1. Bragg's law for X-ray diffraction. The diffracted X-rays exhibit constructive interference when the distance between paths ABC and A'B'C' differs by an integer number of wavelengths (λ).

In this thesis the value of the FWHM (full width at half maximum) of the most intensive line of each phase was used in order to measure the mean particle (crystallite) size, by applying the Scherrer formula:

$$d_{hkl} = (0.9\,\lambda)/\beta\cos\theta \qquad (2)$$

where:

d(hkl) = size (nm) of particles in the direction vertical to the corresponding lattice plane.

λ = X-ray incident wavelength.

β = line broadening at half maximum intensity (FWHM) expressed in rad.

θ = incident angle.

2.2 X-ray Photoelectron Spectroscopy (XPS)

X-ray Photoelectron Spectroscopy is a surface chemical analysis technique based on monitoring the energy of electrons emitted by a system under stimulation of X-rays. X-ray Photoelectron Spectroscopy (XPS) using soft X-ray (200-2000 eV) radiation is mainly to examine core levels. Photoelectron spectroscopy is based upon a single photon in/electron out process. The energy of a photon is given by the Einstein relation:

$$E = h\nu \quad (3)$$

where h is the Planck constant (6.62·10-34 J·s), and ν is the frequency (Hz) of the radiation. Photoelectron spectroscopy uses monochromatic sources of radiation (i.e. photons of fixed energy). In XPS the photon is absorbed by an atom in a molecule or solid, leading to ionization and the emission of a core (inner shell) electron. The kinetic energy distribution of the emitted photoelectrons (i.e. the number of emitted photoelectrons as a function of their kinetic energy) can be measured using any appropriate electron energy analyser and a photoelectron spectrum can thus be recorded. Knowing the kinetic energy of the emitted electrons (KE), the electron binding energy (BE) of each of the emitted electrons can be determined as a difference between the energy of the primary photon (hν) and the kinetic energy of the photoelectron:

$$KE = h\nu - BE \quad (4)$$

The positions of the peaks in the XPS spectrum plotted as emission intensity vs. the electron binding energy gives the information about the atomic composition of the sample surface. Furthermore, the intensity of the peaks is related to the concentration of the element within the sampled region. Thus, the technique provides a quantitative analysis of the surface composition and is sometimes known by the alternative acronym, ESCA (Electron

Spectroscopy for Chemical Analysis). The most commonly employed X-ray sources are those giving rise to: Mg Kα radiation: hν = 1253.6 eV Al Kα radiation: hν= 1486.6 eV.

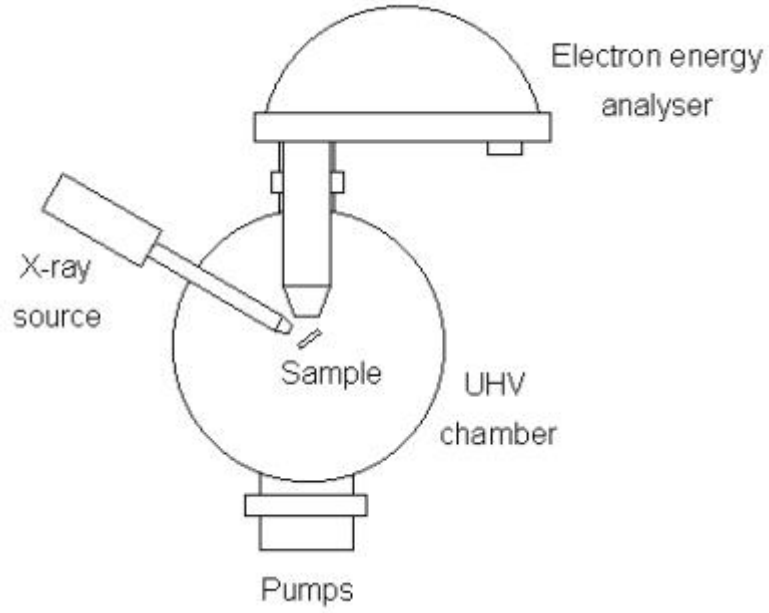

Figure 2.2. Basic scheme of XPS instrumentation

2.3. UV-vis Diffuse Reflectance Spectroscopy (DRS UV-vis)

Diffuse Reflectance Spectroscopy is based on the interaction between a UV or visible beam and a powdered sample, from which the beam can be reflected in all directions. Only the fraction of beam which is scattered within a sample and returned to the surface is considered to be a diffuse reflection. All the reflected radiation can thus be collected within an integrating sphere, enhancing the signal-to noise ratio. The internal walls of the sphere are usually covered with barium sulfide, a compound that ensures a reflectivity greater than 0.98 in the UV-vis light region. Moreover the reflectance spectrum of a reference standard ($BaSO_4$) should always be recorded prior to that of any other sample.

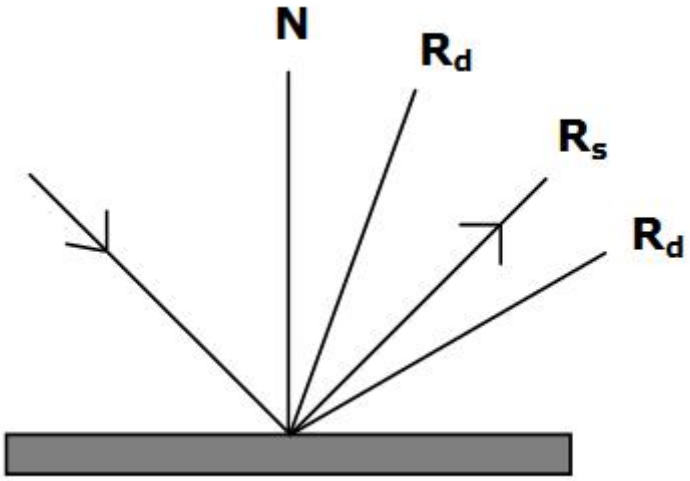

Figure 2.3. Schematic representation of the radiation interaction with the sample: Rs stands for the specular reflected beam, Rd for the diffuse reflected beam

In the literature on photocatalysis, a photoabsorption spectrum, i.e. a plot of the absorption extent as a function of wavelength, is usually reported in terms of absorbance units or Kubelka–Munk function. The former, i.e. absorbance, is traditionally defined as $\log(I_0/I)$, where I_0 and I are the intensities of incident and transmitted light, respectively.

2.4. N_2 sorption analysis

Surface area and porosity are important parameters in powdered materials. The most widely used techniques for estimating surface area are based on physical adsorption of gas molecules on a solid surface. Generally gas adsorption on solid surfaces and in the pore spaces is a complex phenomenon involving mass and energy interaction and phase changes. Depending upon the strength of the interaction, all adsorption processes can be divided into the categories of chemical or physical adsorption. The second category, reversible or physical adsorption, exhibits characteristics that makes it most suitable for surface area determinations as indicated by the following:

• Physical adsorption is accompanied by low heats of adsorption with no violent or disruptive structural changes occurring on the surface during the adsorption measurements.

• Unlike chemisorption, physical adsorption may lead to surface coverage by more than one layer of adsorbate. Thus, pores can be filled by the adsorbate for pore volume measurements.

• At elevate temperatures physical adsorption does not occur or is sufficiently slight that relatively clean surfaces can be prepared on which to make accurate surface area measurements. • Physical adsorption equilibrium is achieved rapidly since no activation energy is required as in chemisorption. An exception here is adsorption in small pores, where diffusion can limit the adsorption rate.

• Physical adsorption is fully reversible, enabling both the adsorption and desorption processes to be studied.

• Physical adsorbed molecules are not restrained to specific sites and are free to cover the entire surface. For this reason surface areas, rather than the number of sites, can be calculated.

The kinetics and thermodynamics of adsorption have been extensively studied, but, when surface area and pore structure are the subject of interest, it's essential to establish the meaning of an adsorption (desorption) isotherm. This is a measure of the molar quantity of gas n (or standard volume Vα, or general quantity q) taken up, or released, at a constant temperature T by an initially clean solid surface as a function of gas pressure P. In order to increase the amount of physisorbed molecules (usually nitrogen) most frequently the test is conducted at a cryogenic temperature, usually that of liquid nitrogen (LN_2) at its boiling point (77.35 K at 1 atm pressure). Convention has established that the quantity of gas adsorbed is expressed as its volume at standard temperature and pressure conditions (0°C and 760 torr and denoted by STP), while the pressure is expressed as a relative pressure, which is the actual gas pressure P divided by the vapor pressure P0 of the adsorbing gas at the temperature of the test. Plots of Vα as the ordinate against P/P0 as the abscissa reveal much about the structure of the adsorbing material (called the adsorbent) simply from their

shape. The theory mainly used in order to get essential information (such as surface area and pore distribution) from experimental adsorption isotherm is known as BET theory from the surnames of its creators, Brunauer, Emmett and Teller [126]. This is an extension to multilayer adsorption of the Langmuir model (related to monolayer molecular adsorption) and the resulting BET equation is expressed as follows:

$$V_\alpha = (V_m CP)/ (P_0-P) [1+ (C-1) (P/P_0)] \quad (5)$$

where:

V_α = volume of adsorbed gas at pressure P.

V_m = monolayer volume.

P = gas pressure.

P_0 = saturation gas pressure. The value of parameter C, fairly constant for a given class of materials, e.g. oxides and metals, in simplest terms is given by the following equation:

$$C \alpha \exp [(q_1-q_L)/RT] \quad (6)$$

where:

q_1 = heat of adsorption of the first layer.

q_L = heat of liquefaction of the adsorptive.

R = gas constant.

T = absolute temperature.

From the slope and intercept values of the BET linear plot it is possible to calculate both the amount of adsorbate corresponding to the first monolayer, Vm, and the C parameter can be calculated. Assuming that the surface occupied by a N_2 molecule is

16.2·10-20 m^2, once calculated V_m, it's easy to obtain the Specific Surface Area (SSA) of the adsorbing material, by the following equation:

$$SSA = (Vm\ N_A\ S_{N2}) / 22.414\ g \quad (7)$$

where:

N_A = Avogadro number (6.023·1023 molecules mol^{-1}).

S_{N2} = surface occupied by a N_2 molecule adsorbed on the monolayer.

22.414 = volume (dm^3) occupied by 1 mole of gas under standard conditions.

g = sample quantity (g).

2.5. Electron microscopy

Electron Microscopes are scientific instruments that use a beam of highly energetic electrons to examine objects on a very fine scale. This examination can yield information about the topography (surface features of an object), morphology (shape and size of the particles making up the object), composition (the elements and compounds that the object is composed of and the relative amounts of them) and crystallographic information (how the atoms are arranged in the object).

When an electron beam interacts with the atoms in a sample, individual incident electrons undergo two types of scattering - elastic and inelastic. In the former, only the trajectory changes and the kinetic energy and velocity remain constant. In the case of inelastic scattering, some incident electrons will actually collide with and displace different kind of electrons from the specimen, thus loosing their kinetic energy. Figure 2.4. summarizes the main secondary signals (with different relative intensity) that can be produced due to electron–matter interactions [127]. TEM instruments must work under ultra

high vacuum conditions (10^{-7}-10^{-8} Pa) in order to avoid any kind of collision between the electrons beam and atoms, which are not those contained in the investigated sample.

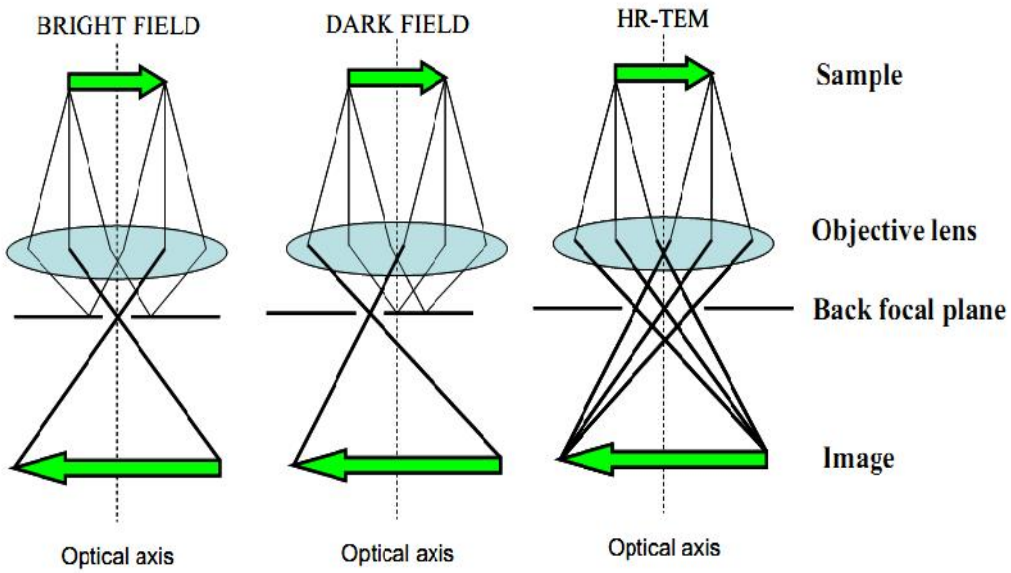

Figure 2.4. Generalized description of the three main imaging modes in TEM

Chapter 3

Experimental Section

3.1. Synthesis of catalyst

Cadmium nitrate tetra hydrate, ceric nitrate and thiourea were purchased from Merck and used as received. Different molar ratios of cerium and cadmium precursors (0.1:1, 0.5:1, 1:1, 1:0.5 moles of cadmium and cerium precursors respectively) were taken in order to obtain the composites with best characteristics. In an optimized synthesis, aqueous solutions of cadmium nitrate, cerium (IV) nitrate and thiourea were mixed to form a homogeneous solution. Dehydration followed by combustion in a preheated furnace at 350° C results the product in few minutes. The resulting composites were labeled as CdS/CeO_2 (0.1:1), CdS/CeO_2 (0.5:1), CdS/ CeO_2 (1:1)), CdS/ CeO_2 (1:0.5) respectively. The specific advantage of the present method is the fast reaction time and the samples do not need any post treatments before testing catalytic activity.

3.2. Instruments Used

The synthesized CdS/CeO_2 composites were characterized to examine its structural, morphological and optical properties. Phase purity and crystallinity of the as-synthesized composites was obtained from wide angle powder X-ray diffraction (PXRD) patterns recorded on a PANalytical X'pert Pro powder X-ray diffractometer with a step size of 0.02 and at a scan rate of 0.50 min^{-1} using Cu-Kα (1.54 Å) radiation and Ni filter. Transmission electron microscopic image of the CdS/ CeO_2 samples were recorded at an operating voltage of 200 kV and the sample was placed on a copper grid (TECNAI G-2 with EDS model), whereas, diffuse UV-Vis reflectance spectra of the prepared composite samples were

collected using Shimadzu UV-Vis spectrophotometer (UV-3600) with a spectral grade $BaSO_4$ as reference. X-ray photoelectron spectroscopic study was performed on Axis Ultra instrument under ultra-high vacuum condition ($<10^{-8}$ Torr) and by using a monochromatic Al Kα X-ray source (1486.6 eV). The source power of XPS instrument was maintained at 150 W and the emitted photoelectrons were sampled from 750 μm x 300 μm area. The analyzer pass energy was 80 eV for survey spectra and 40 eV for high-resolution spectra. Raman spectra of the as synthesized samples were recorded using a dispersive Raman spectroscope (Bruker Senterra), whereas, nitrogen adsorption/desorption isotherms of the CdS/ CeO_2 nano hetero structures were recorded on a Quantachrome autosorb automated gas sorption system (NOVA 2200 e). Prior to adsorption studies, the samples were degassed at 573 K for 3 h. The Brunauer–Emmett–Teller (BET) equation was used to determine the surface area from the adsorption isotherm.

Photocatalytic experiments were carried out in a photo reactor which consists of three 250 W halogen lamps. The intensity of light falling on the sample cells was found to be 850-900 W/m^2 as measured by using Newport optical power/energy meter (Model 842. PE).Visible light activity of the TiO_2 samples was assessed by simultaneous and individual study of oxidation of phenol and reduction of Cr(VI) from aqueous streams. Before exposing to light source the sample solutions along with catalysts were allowed to attain adsorption desorption equilibrium by stirring in dark for a period of 30 min. Experiments were carried out in the absence of light and without catalyst and it was observed that there was no considerable oxidation of phenol or reduction of Cr(VI). During the light exposure for every 15 min small aliquots were collected, centrifuged at an rpm of 2000 and the catalysts particles were separated by filtering with milli Q membrane filters. Thereafter phenol and Cr(VI) were estimated by using UV-Vis spectrophotometer.

Before spectrophotometric analysis, phenol was converted into a complex by adding 1ml of buffer (pH-9) followed by 1 ml of 0.05 M 4-aminoantipyrene and 1ml of 0.05 M

potassium ferricyanide aqueous solution [128,129]. Then the obtained brownish red antipyrene dye was estimated with UV-Vis Spectrometer (Shimadzu UV-Vis spectrophotometer (UV-3600)) at 504 nm. Cr(VI) was estimated by forming a purple coloured complex with 1, 5- Diphenyl hydrazide solution in acidic media [130]. The concentration of Cr(VI) was estimated from the absorbance at 540 nm by using UV-Vis spectrophotometer.

H_2 production experiments were carried out under visible irradiation in a quartz round bottomed flask containing 100 ml water and 100 mg of the catalyst. A solution containing 1 M Na_2S and 1M Na_2SO_3 was used sacrificial source. It has been observed that there is no H_2 production in the dark which confirms that there is no reaction in the dark. All the studies were carried out under simulated visible light radiation with light intensity around 800-900 W/m^2, as measured by Newport power meter. At regular intervals the produced H_2 gas was analyzed by using a Shimadzu gas chromatography (GC-2014) with a packed column. Every hour a 500 µl hydrogen gas was collected in a gas tight syringe (Hamilton) and analyzed.

Chapter 4

Results and Discussion

4.1. XRD

Figure 4.1. shows the XRD patterns of CdS/ CeO_2 composites along with pure CeO_2 and CdS samples for comparison. It was observed that the peaks observed at 2θ of 28.5, 33.1, 47.4 and 56.3° with the corresponding d-spacing of 3.1, 2.7, 1.9 and 1.6 Å represent (111), (200), (220) and (311) planes, respectively of cubic structure of CeO_2 (PCPDF No. 810792). On the other hand for pure CdS, the peaks observed at 28.2, 24.8, 43.7, 26.5 and 47.9° corresponding to 101, 100, 110, 002 and 103 planes with the corresponding d-spacing values of 3.6, 3.4, 3.2, 2.1 and 1.9 Å clearly indicate the existence of hexagonal CdS phase. It was observed that all the composites have the peaks corresponding to the both fluorite cubic phase CeO_2 and hexagonal CdS phases with varying intensities which confirms the coexistence of both the phases. The dotted lines in the figure correspond to the diffraction peaks of hexagonal CdS whereas the dark lines indicated that of cubic phase CeO_2. In the case of CdS/ CeO_2 (0.5:1) the XRD patterns shows rather weak CdS peaks, probably due to the low loading of CdS. A similar observation was found in case of CdS/ CeO_2 (1:0.5) where the XRD pattern showed rather weak CeO_2 peaks which may be due to the low amount of CeO_2. On the other hand, for CdS/ CeO_2 (1:1), diffraction peaks corresponding to

both CeO_2 and CdS were observed, which can be attributed to the proper dispersion and optimum loading of CdS on CeO_2.

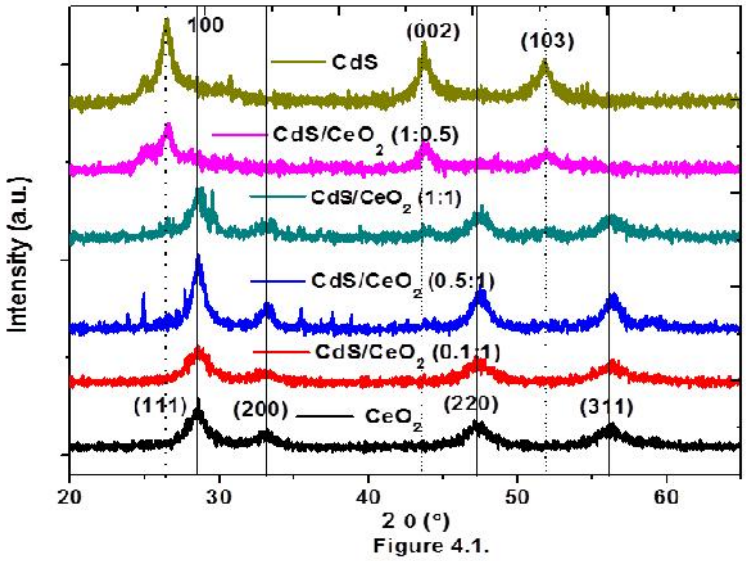

Figure 4.1.

4.2. TEM

Figure 4.2. shows the TEM image of the CdS/CeO_2 (1:1) sample which clearly shows the presence of two distinct particles with different size. It also shows closely connected CdS and CeO_2 particles. This clearly shows the advantage of the present synthesis. As observed from figure 2, the CeO_2 particles have a size of around 10 nm whereas CdS particles have relatively larger size of around 70 nm. In the HRTEM images of the CdS/ CeO_2 (Fig. 4.2.(b)), confirmed the formation of crystalline CeO_2 and CdS. The fringes with a lattice spacing of 0.27 and 0.33 nm for the CdS/ CeO_2 composites (Fig. 4.2. (b)) were assigned to (200) and (100) planes of cubic CeO_2 (JCPDS file No. 65-2975) and hexagonal CdS (JCPDS file No. 77-2306), respectively.

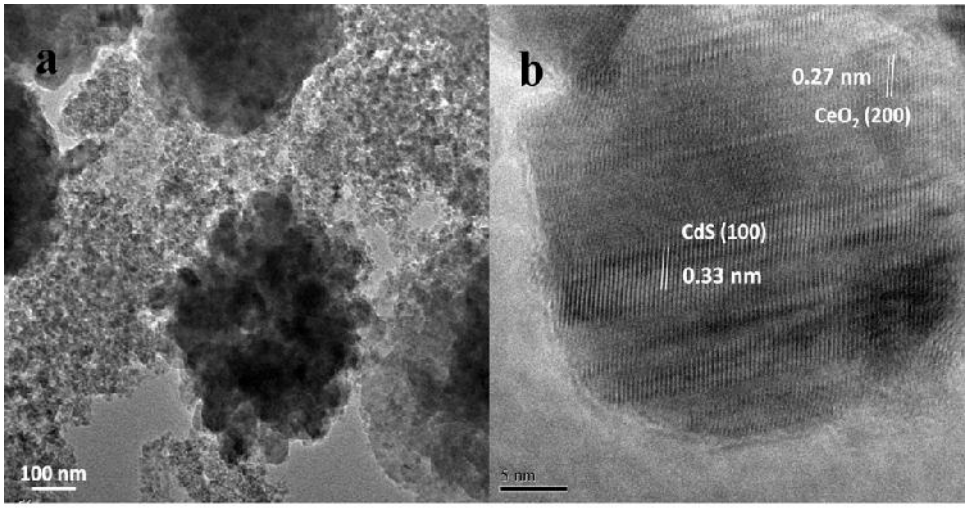

Figure 4.2.

4.3. Diffuse reflectance UV-Vis spectral studies

The composite nature of CdS/CeO_2 may be further evidenced by the diffuse reflectance UV−vis spectra as shown in figure 4.3. Pure CeO_2 only absorbs in the UV region with a band edge of approximately 400 nm (Eg = 3.2 eV). But the composite sample exhibited two distinct absorption edges corresponding to CeO_2 (around 380-400 nm) and a strong absorbance in the visible light region CdS (around 550-570 nm). The studies show that the CdS/ CeO_2 hetero nano structures absorbs in the visible as well as in the UV region of the solar spectrum.

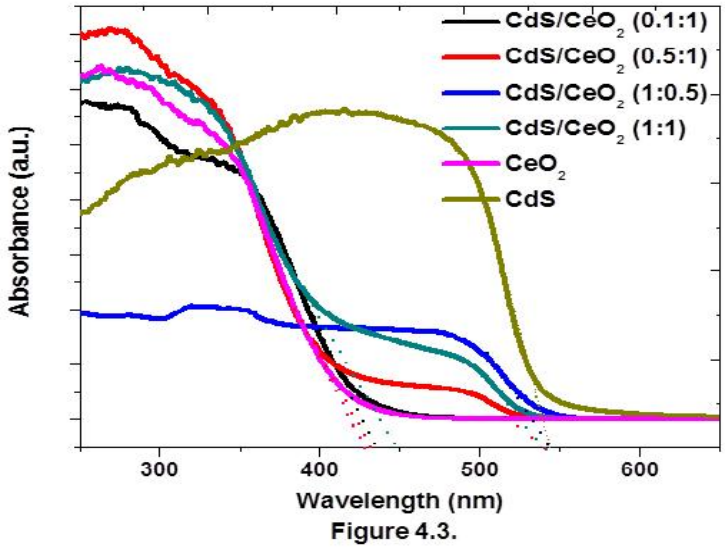

Figure 4.3.

4.4. Raman Spectroscopy

It has been accepted that Raman spectroscopy is a powerful technique for the investigation of the structural properties of nanoparticles. Decreasing particle size influences the force constants and vibrational amplitudes. Figure 4.4. shows the Raman spectra of the CdS/ CeO_2 hetero nanostructure where dotted lines indicate the peaks corresponding to the CdS and solid lines represents the peaks corresponding to the CeO_2. For pure CeO_2 sample a strong peak at 464 cm^{-1} was observed which can be assigned to F2g Raman active interior phonon mode of CeO_2 fluorite structure [44, 45], and can be viewed as a symmetric breathing mode of the oxygen atoms around Ce^{4+} ions [46]. One more peak which was observed at around 600 cm^{-1} for pure CeO_2 may be due to the presence defect induced oxygen vacancies (D-band) on the surface [44-46]. From figure 4.4. it is also clear that the Raman peaks at 300 cm^{-1} and 600 cm^{-1} for pure CdS correspond to the first-order and second order transverse optical phonon modes [62]. The relatively broad and symmetric nature of Raman peaks of CdS indicates the lower crystallinity of CdS, which is also consistent with the XRD observations. The intensity of Raman peaks for CdS/ CeO_2 hetero nanostructures is lower than either pure CeO_2 or pure CdS. This may be attributed to scattering losses due to the defects at the hetero junction. In all the CdS/ CeO_2 composites (Except in case of CdS/CeO_2(0.1:1)) Raman peaks corresponding to CdS are predominant, probably due to the high dispersion of CdS over CeO_2.

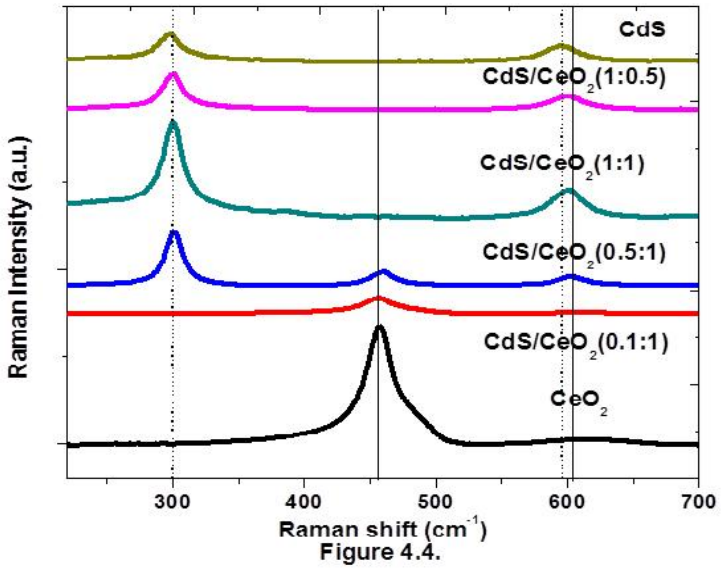

Figure 4.4.

4.5. XPS

The presence of Ce, Cd, O, S, C and N elements in the CdS/ CeO_2 composites and their surface composition, valence states were determined by using XPS. Figure 4.5. depicts the XPS spectra of Ce 3d, Cd 3d, S 2p, O1s, C 1s and N 1s core levels. As seen in figure 4.5.(a), the two peaks centered at 405.2 and 412.1 eV with a spin−orbit separation of 6.7 eV were the characteristic peaks of Cd $3d_{5/2}$ and Cd $3d_{3/2}$ states of CdS which are consistent with the reported values [134-137]. On the other hand, the peaks centered at 161.5 eV and 162.7 eV confirmed the S_{2p} (figure 4.5.(b)) confirming the presence of sulfur in the non-oxidized form.

Ce 3d core level spectra of these solid solutions are given in figure 4.5.(c). Since the signal of the Ce 3d level has a very complicated satellite structure, the origins of the bands for cerium are still under investigation [138–140]. According to the method that Burroughs et al. established [141] the Ce 3d XPS peaks shown in figure 4.5.(c) are labeled for identification, where the peaks labeled v and u are from the spin–orbit coupling $3d_{5/2}$ and $3d_{3/2}$, respectively. The peaks of v, v'' and v''' correspond to a mixing configuration of Ce(IV) ($3d^9 4f^2$) O($2p^4$), Ce(IV) ($3d^9 4f^1$) O($2p^5$) and Ce(IV)($3d^9 4f^0$) O($2p^6$), respectively. The peaks v_o and v' are assigned to a mixture of Ce(III) ($3d^9 4f^2$) O($2p^5$) and Ce(III)

($3d^9 4f^1$)O($2p^6$), respectively. The same assignments could be also applied to the u series of peaks. In figure 4.5.(c), Ce3d spectrum of Ce(IV) has six peaks at the binding energies of 916.5, 907.5,900.9, 897.7, 889.3, and 882.4 eV, respectively. Among these peaks the peak at 889.3 eV corresponds to the v' of Ce(III) whereas the remaining represents the characteristic peaks for Ce(IV) oxidation state. Figure 4.5.(d) shows the O1s spectra with a narrow peak at a binding energy of 530.4 eV can be attributed to the crystal lattice oxygen of Ti−O.

The evidence of C doping was obtained from the deconvoluted spectrum (figure 4.5.(e)) from the peaks centered at 284.5 eV and 288.5 eV. The peak centered at 284.5 eV was due to elemental carbon, whereas, the peak at 288.5 eV may be due to the carbonate type of linkages. Sakthivel and Kwasch et. al. has reported two kinds of carbonate species at binding energies of 287.5 and 288.5 eV [142]. In a similar manner, Ohno et al. detected only one kind of carbonate species with a binding energy of 288.0 eV, and they concluded that C^{4+} ions might be incorporated into the bulk phase of TiO_2 [143]. Li et al. confirmed only one kind of carbonate species at a binding energy of 288.2 eV [144], which is confirmed by Ren et al. [145]. These results indicated that the peak at 288.5 eV in the C 1s spectrum may be attributed to the O=C–O components [146].

The evidence for nitrogen doping was obtained from the N (1s) spectra, which clearly show two peaks at 399.7 eV and 405 eV (figure 4.5.(f)). It is well known that the binding energy of the N 1s is very sensitive to the chemical environment of the nitrogen and it varies between 396-408 eV [147]. The peaks observed at 399.7 eV can be attributed to the terminally bonded well screened molecular nitrogen (γ-N_2), whereas, the 405 eV peak might be due to terminally bonded poorly screened molecular nitrogen (γ-N_2) [148].

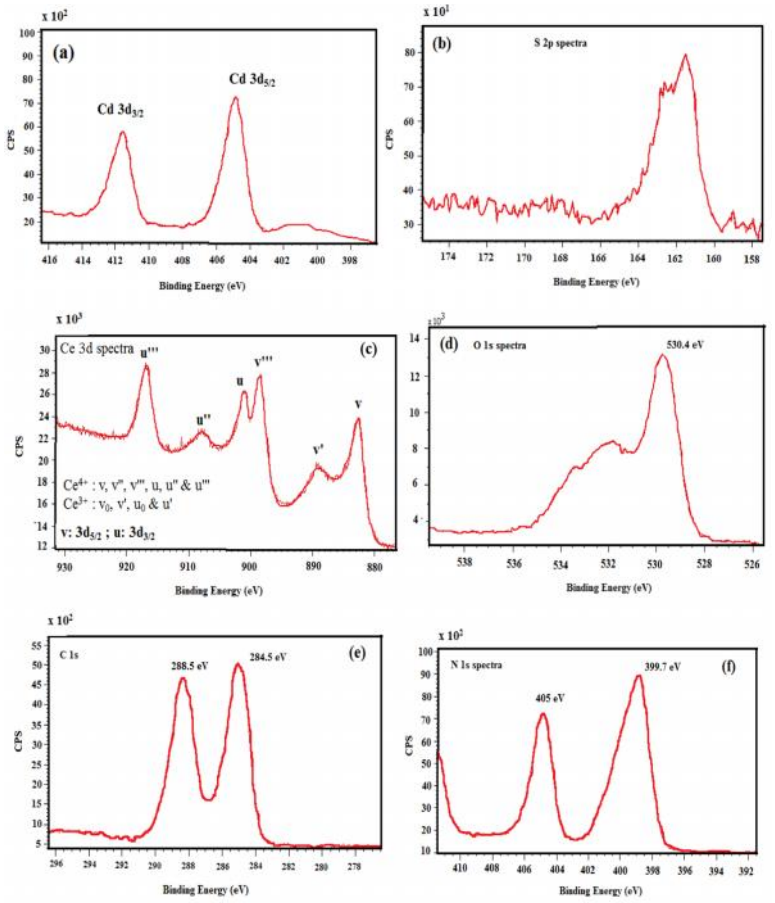

Figure 4.5.

4.6. N_2 adsorption studies

The specific surface area of the CdS/ CeO_2 samples was obtained from the N_2 adsorption-desorption isotherms by using BET method. The observed specific surface area values are found to be 10, 18, 23, 27, 32, 8 m^2g^{-1} for CdS/ CeO_2 (0.1:1), CdS/ CeO_2 (0.5:1), CdS/ CeO_2 (1:1), CdS/ CeO_2 (1:0.5), CdS, CeO_2 respectively. From these, it may be concluded that pure CdS has more surface area than the composites and among the composites CdS/ CeO_2 (1:0.5) have higher surface area which of can be attributed to the higher percentage CdS than CeO_2.

4.7. Photocatalytic Studies

The improved visible light absorption and benefit of reduced exciton recombination may be beneficial for the composites to show promising photocatalytic activity. In order to

understand this, photocatalytic activity was assessed for oxidation of phenol and reduction of Cr (VI) as model aqueous organic pollutants and the results are compared with standard Evonik TiO_2. Figure 4.6. shows the first order kinetic profiles of photocatalytic reduction of 100 ppm of Cr(VI) in the presence of all the photocatalysts. The first order rate constants calculated from the slopes as shown in figure 4.6. are found to be 0.11, 0.14, 0.19, 0.16, 0.1, 0.04, 0.02 min^{-1} respectively for CdS/CeO_2 (0.1:1), CdS/ CeO_2 (0.5:1), CdS/ CeO_2 (1:1), CdS/ CeO_2 (1:0.5), CdS, CeO_2 (tu) and Evonik TiO_2, highlighting the best activity of CdS/ CeO_2 (1:1) and the activity was in the following order: CdS/ CeO_2 (1:1) > CdS/ CeO_2 (1:0.5) > CdS/ CeO_2 (0.5:1) > CdS > CeO_2 (tu) > Evonik TiO_2.

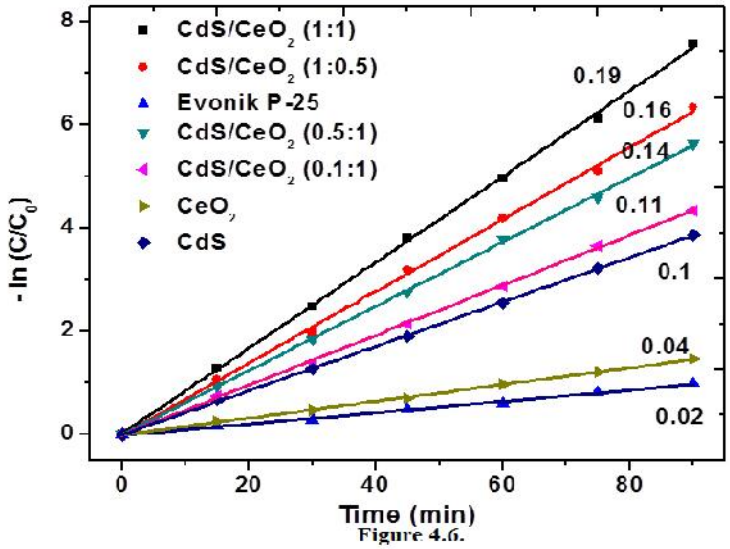

Figure 4.6.

In order to understand the effect of concentration on photocatalytic reduction of Cr(VI) photocatalytic studies were carried out with different concentration of Cr(VI) such as 25, 50,75 and 100 ppm. Figure 4.7. shows the first order rate plots for the phtocatalytic reduction of Cr(VI). The rate constants calculated from the slopes of first order plots were found to be 0.15, 0.18, 0.23 and 0.28 min^{-1} respectively for 100, 75, 50 and 25 ppm of Cr(VI). From these observations it is concluded that with increase of initial concentration of Cr(VI) the rate constant decreases gradually. This can be explained based on the hindering effect imposed with the increasing concentration of Cr(VI), which prevents the photons to

reach the surface of photocatalyst [149]. In addition to this, with increasing concentration of Cr(VI), the molecules adsorbed on the surface of photocatalyst might increase. This might decrease the active sites on the photocatalyst which effects the generation of hydroxyl radical, and hence lowers the activity [149].

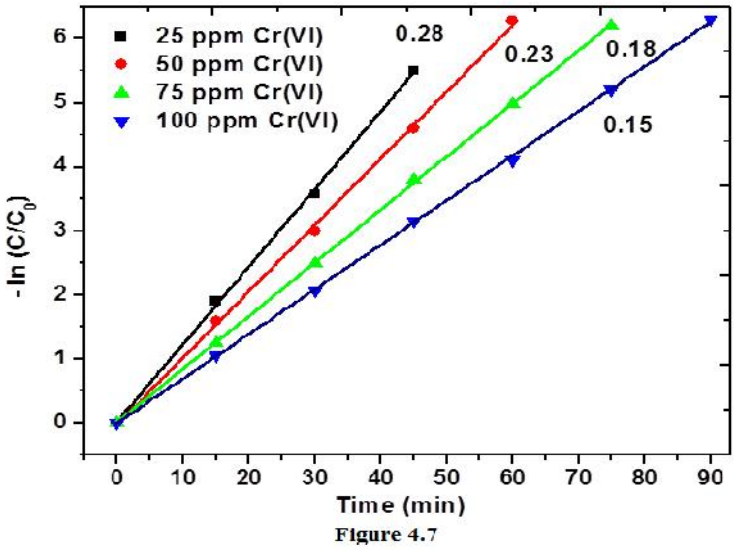

Figure 4.7

4.7.1. Photocatalytic oxidation of phenol

The effect of phenol concentration on the activity of the photocatalyst is presented in Fig. 4.8. Concentrations were tested between 20 and 50 ppm using 1 g/L of catalyst. It has been observed that with increasing concentration of phenol rate constant decreases. The rate constants observed are found to be 0.38, 0.32, 0.28 and 0.22 min^{-1} respectively for 20, 30, 40 and 50 ppm of phenol. This can be explained as follows: At higher concentration of phenol, there might be a greater number of phenol molecules adsorbed on the surface and they may form a “passive” monolayer [150]. This inhibits additional phenol molecules to reach the CdS/CeO_2 surface, hence, the reduction in photocatalytic degradation.

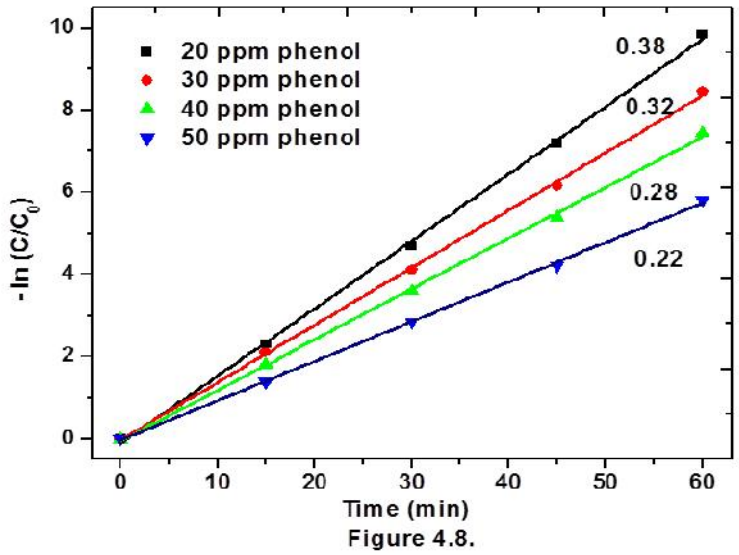

Figure 4.8.

4.7.2. Simultaneous oxidation of phenol and reduction of Cr(VI)

Since the industrial waste water consists of mixture of pollutants, simultaneous oxidation and reduction of phenol and Cr(VI) respectively may be advantageous. In addition, simultaneous treatment reduces the cost of the water treatment. Figure 4.9. shows the first order kinetic plots for the simultaneous oxidation and reduction of phenol and Cr(VI), respectively. 50 ppm of Cr(VI) aqueous solution and 30 ppm of phenol were taken as a combination of pollutants. It is worth mentioning that there is no reaction in the dark or without catalyst. From the rate constants, it is concluded that in case of simultaneous reaction the rate constant was found to be two times higher than individual reactions, which can be explained based on the plausible mechanism as described in the following sections. Therefore simultaneous redox reactions not only decreases the water treatment cost but also increases the efficiency of the reaction.

High activity of CdS/ CeO_2 composites compared to the bare CdS and CeO_2 can be attributed to the electron transfer from CdS to CeO_2 since the conduction band edge of CdS is higher than that of CeO_2. Under visible light irradiation CdS undergo excitation and the photo generated electrons transfer from the conduction band of CdS to CeO_2 and

accumulate at the lower level conduction band of CeO_2, while holes accumulate at the valence band of CdS. Thus the exciton recombination can be prevented effectively.

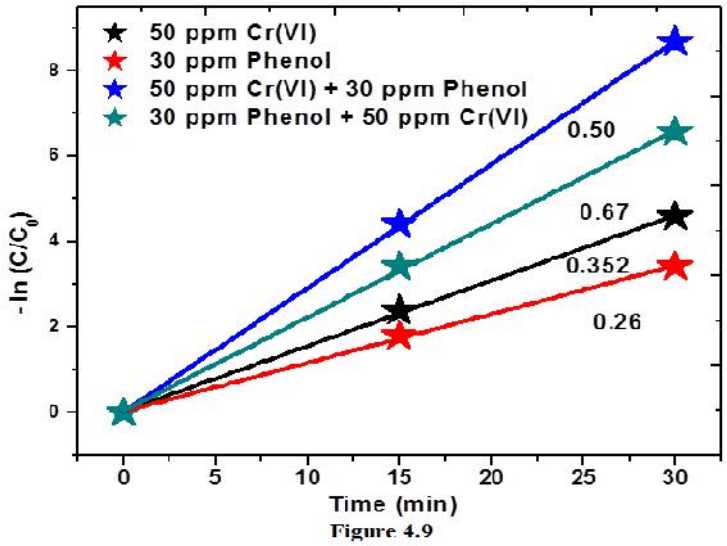

Figure 4.9

4.7.3. Photocatalytic H_2 production from water

Since all the composites are found to have good absorption in the visible region of the solar spectrum, the visible light activity of the CdS/CeO_2 photocatalysts were tested for hydrogen production from water containing sacrificial agents. In order to reduce the photocorrosion of CdS and to prevent further the recombination of excitons, water containing 1M Na_2S and 1M Na_2SO_3 as the sacrificial reagents was used. These sacrificial reagents may interact with the holes that prevent the photocorrosion of CdS catalyst[39]. During the photocatalytic reaction for every one hour H_2 gas was collected by using a gas tight syringe and analyzed by gas chromatography. The typical chromatogram observed was shown in Fig S5 of supporting information. H_2 production studies were carried out with all the CdS/CeO_2 samples along with pure CdS and CeO_2 for comparison. The typical results shown in figure 4.10. confirmed the formation of 504, 789, 1581, 2144, 2315 and 2778 µ mol/h of hydrogen, respectively for CeO_2 (1), CdS/ CeO_2 (0.1:1), CdS/ CeO_2 (0.5:1), CdS, CdS/ CeO_2 (1:0.5) and CdS/ CeO_2 (1:1) respectively. These results confirmed that the highest hydrogen evolution was achieved for CdS/ CeO_2 (1:1).

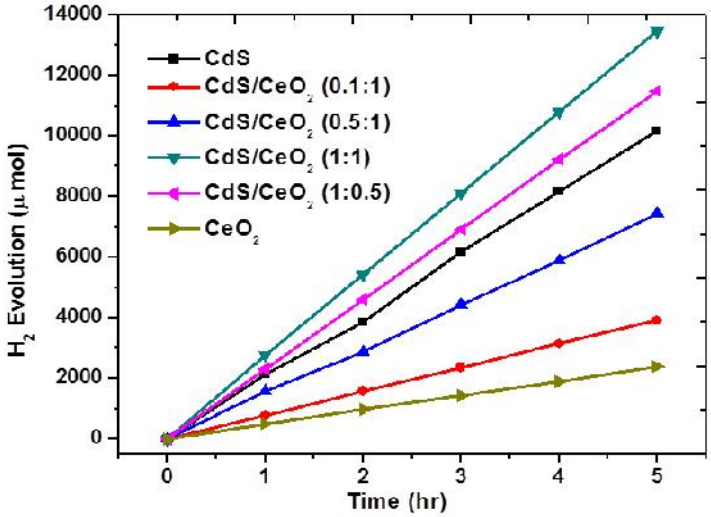
14000
12000
10000
8000
6000
4000
2000
0
H2 Evolution (μmol)
0
1
2
3
4
5
Time (hr)
CdS
CdS/CeO2 (0.1:1)
CdS/CeO2 (0.5:1)
CdS/CeO2 (1:1)
CdS/CeO2 (1:0.5)
CeO2

Figure 4.10.

Chapter 5

Conclusions

In summary, a single step synthesis of CdS/ CeO_2 hetero nanostructures by combustion synthesis without using expensive surfactants and capping agents has been reported. Various physico-chemical studies confirmed the formation of CeO_2 and CdS, and confirmed the best adsorption in the visible region. Photocatalytic activity of the composites was assessed from the simultaneous oxidation of phenol and reduction of Cr(VI), whereas, photocatalytic water splitting without the need of any noble metal indicated the promising nature of CdS/ CeO_2 system for H_2 production.

References

[1] A. M. Omer. Green energies and the environment Review Article. Renew. Sustain. Energ. Rev. 12, (2008) 1789-1821.

[2] I. Dincer and M. A. Rosen. Energy, environvent & sustainable development. Appl. energ. 64, (1999) 427-440.

[3] I. Dincer. Environmental impacts of energy. Energ. Policy. 27, (1999) 845-854.

[4] A. Midilli, I. Dincer and M. A. Rosen. On hydrogen and hydrogen energy strategies: I: current status and needs. 9, (2005) 255–271.

[5] J. W. Gosselink. Pathways to a more sustainable production of energy: sustainable hydrogen—a research objective for Shell. 27, (2002) 1125–1129.

[6] A. Demirbas. Biomass resource facilities and biomass conversion processing for fuels and chemicals. 42, (2001) 1357–1378.

[7] D. Das and T. N. Veziroglu. Hydrogen production by biological processes: a survey of literature. Int. J. Hydrogen Energ. 26, (2001) 13-28.

[8] I. Dincer. Renewable energy and sustainable development: a crucial review. 4, (2000) 157–175.

[9] John Harte. Human population as a dynamic factor in environmental degradation, Popul. Environ. 28, (2007) 223–236.

[10] M. Valcarcel, S. Cardenas, B.M. Simonet, Y. M.-Martınez and R. Lucena, Carbon nanostructures as sorbent materials in analytical processes. Trends in Analy. Chem. 27, (2008) 34-43.

[11] L.-S. Zhong, J.-S. Hu, H.-P. Liang, A.-M. Cao, W.-G. Song and L.-J. Wan. Advan. Mater. 18, (2006) 2426-2431.

[12] Z.-G. Wang, L.-S. Wan, Z.-M. Liu, X.-J. Huang and Z.-K. Xu. Enzyme immobilization on electrospun polymer nanofibers: An overview. J. Molec. Catal. B: Enzymatic. 56, (2009) 189–195.

[13] P. K. Chattaraj, S. Bandaru and S. Mondal. Hydrogen Storage in Clathrate Hydrates. J. Phys. Chem. A. 115, (2011) 187–193.

[14] David B. Levina and Richard Chahine. Challenges for renewable hydrogen production from biomass. Int. J. Hydrogen Energ. 35, (2010) 4962–4969.

[15] M. Ni, D. Y.C. Leung and M. K.H. Leung. A review on reforming bio-ethanol for hydrogen production. Int. J. Hydrogen Energ. 32, (2007) 3238 – 3247.

[16] P.P. Edwards , V.L. Kuznetsova, W.I.F. David and N.P. Brandon. Hydrogen and fuel cells: Towards a sustainable energy future. Energy Policy. 36, (2008) 4356–4362.

[17] J.D. Holladay, J. Hu, D.L. King and Y. Wang. An overview of hydrogen production technologies. Catalysis Today. 139, (2009) 244–26 .

[18] M. Balla and M. Wietschel. The future of hydrogen – opportunities and challenges. Int. J. Hydrogen Energ. 34, (2009) 615–627.

[19] J. N. Armor. The multiple roles for catalysis in the production of H_2. Appl. Catal. A: Gen. 176, (1999) 159-176.

[20] J. J. Burke, C. Sauveplane and M. M. President. Groundwater management and socio-economic responses. Natural Resources Forum. 23, (1999) 303–313

[21] A. K. Kivaisi. The potential for constructed wetlands for wastewater treatment and reuse in developing countries: a review. Ecological Engineering. 16, (2001) 545–560.

[22] B. Jiménez. Irrigation in Developing Countries Using Wastewater. Int. Rev. Environ. Strateg. 6, (2006) 229 – 250.

[23] Len Ritter, Keith Solomon, Paul Sibley, Ken Hall, Patricia Keen, Gevan Mattu, Beth Linton, Sources, pathways, and relative risks of contaminants in surface water and ground water: A perspective prepared for the walkerton Inquiry. J. Toxicol. Environ. Health, Part A: Current Issues. 65(2002) 1-9.

[24] R. Maria. Saleth and Ariel Diner. Institutional changes in global water sector: trends, patterns, and implications. 2, (2000) 175–199.

[25] A. M. Omer. Green energies and the environment Review Article Renewable and Sustain. Energ. Rev. 12, (2008) 1789-1821.

[26] A. J. B. Zehnder, H. Yang and R. Schertenlei. Water issues: the need for action at different levels. Aquat. Sci. 65, (2003) 1–20.

[27] T. A. Ternes , M. M. Heimer , D. Mcdowell , F. Sacher , H. – J. Brauch , B. H. - Gulde, G. Preuss, U. Wilme and N. Z. – Seibert. Removal of Pharmaceuticals during Drinking Water Treatment. Environ. Sci. Technol. 36, (2002) 3855-3863.

[28] O. Legrini, E. Oliveros, and A. M. Braun. Photochemical Processes for Water Treatment. Chem. Rev. 93, (2001) 671-698

[29] A . Hambidge. Reviewing efficacy of alternative water treatment techniques, Health Estate. 55, (2001) 23-25.

[30] T. A. Kurniawan, G. Y.S. Chana, W-H. Lo, S. Babel. Physico–chemical treatment techniques for wastewater laden with heavy metals. Chem. Eng. J. 118, (2006) 83–98.

[31] P.P. Zolotarev, V.V. Ugrozov, I.B. Volkina, V.M. Nikulin, Treatment of waste water for removing heavy metals by membrane distillation. J Haz. Mater. 37, (1994) 77-82

[32] I. Hua and M. R. Hoffmann. Optimization of Ultrasonic Irradiation as an Advanced Oxidation Technology. Environ. Sci. Technol. 31, (1997) 2237–2243.

[33] E. J. Rosenfeldt and K. G. Linden. Degradation of Endocrine Disrupting Chemicals Bisphenol A, Ethinyl Estradiol, and Estradiol during UV Photolysis and Advanced Oxidation Processes. Environ. Sci. Technol, 38, (2004) 5476–5483.

[34] M. Zaw, M. T. Emett. Arsenic removal from water using advanced oxidation processes. Toxicol. Lett. 133, (2002) 113-118.

[35] M. M. Huber , S. Canonica , G.-Y. Park, and U. V. Gunten,. Oxidation of Pharmaceuticals during Ozonation and Advanced Oxidation Processes. Environ. Sci. Technol. 37, (2003) 1016–1024.

[36] N. A. Serpone and A. V. Emeline. "Suggested terms and definitions in photocatalysis and radiocatalysis," Int. J. Photoenerg. 4, (2002) 91-131.

[37] A. Fujishima and K. Honda. Nature. 37, (1972) 238-239.

[38] A. J. Bard. J. Phys. Chem. 86, (1982) 171-75.

[39] M. Gratzel. Energy Resources Through Photochemistry and Catalysis: Academic Press: New York. 1983.

[40] K. Kalyanasundaram, M. Gratzel, E. Pelizzetti. Coord. Chem. Rev. 69, (1986) 57.

[41] V. N. Parmon, K. I. Zamareav. In Photocatalysis -Fundamentals and Applications; Serpone, N., Pelizzetti, E., Eds.: Wiley Interscience: New York. (1989) 565.

[42] E. Pelizzetti, M. Schiavello, Eds. Photochemical Conversion and Storage of Solar Energy: Kluwer Academic Publishers: Dordrecht. 1991.

[43] A. G. Agrios and P. Pichat. J. Appl. Electrochem.. 35, (2005) 655.

[44] M. Gratzel. Nature. 414, (2001) 338-345.

[45] A. L. Linsebigler, G. Lu, and J. T. Yates Jr. Chem. Rev. 95, (1995) 735-745.

[46] M. R. Hofmann, S. T. Martin, W. Choi, and D. W. Bahnemann. Chem. Rev. 95, (1995)69-75.

[47] Y. Tachibana, K. Umekita, Y. Otsuka and S. Kuwabata. J. Phys. Chem. C. 113(2009) 6852-6857

[48] I. Robel, V. Subramanian, M. Kuno and P. V. Kamat. J. Am.Chem. Soc. 128, (2006) 2385-2386.

[49] W. T. Sun, Y. Yu, H. Y. Pan, X. F. Gao, Q. Chen, L. M. Peng, J. Am. Chem. Soc. 130, (2008) 1124−1125.

[50] Y. L. Lee, B. M. Huang, H. T. Chien. Chem. Mater. 20 (2008) 6903−6905.

[51] L. M. Peter, D. J. Riley, E. J. Tull, K. G. Wijayantha, Chem.Commun. (2002) 1030−1031.

[52] L. J. Diguna, Q. Shen, J. Kobayashi, T. Toyoda, Appl. Phys.Lett. 91(2007) 023116-023117.

[53] Y. Bessekhouad, D. Robert, J. V. Weber, J. Photochem.Photobiol. A. 163, (2004) 569−580.

[54] C. Ratanatawanate, C. Xiong, K. J. Jr. Balkus. ACS Nano. 2, (2008) 1682−1688.

[55] X. Y. Gan, X. M. Li, X. D. Gao, J. J. Qiu, F. W. Zhuge. Nanotechnology. 22, (2011) 305601.

[56] H. Tsukigase, Y. Suzuki, M. H. Berger, T. Sagawa, S. Yoshikawa, J. Nanosci. Nanotechnol. 11, (2011)3215−3221

[57] N. Ghows, M. H. Entezari, Ultrason. Sonochem, 18, (2001) 629−634.

[58] M. Nanu, J. Schoonman, A. Goossens, Adv. Funct. Mater. 15, (2005) 95−100.

[59] W. Zhu, X. Liu, H. Q. Liu, D. L. Tong, J. Y. Yang, J. Y. Peng, J. Am. Chem. Soc. 132, (2010) 12619−12626.

[60] H. Tada, T. Mitsui, T. Kiyonaga, T. Akita and K. Tanaka, Nat. Mater. 5(2006) 782–786.

[61] M. Matsumura, S. Furukawa, Y. Saho and H. Tsubomura, J. Phys.Chem., 89, (1985) 1327-1334.

[62] J. F. Reber and K. Meier, J. Phys. Chem. 90, (1986) 824-829.

[63] L. Spanhel, H.Weller and A. Henglein, J. Am. Chem. Soc. 109, (1987) 6632–6635.

[64] P. A. Sant and P. V. Kamat. Phys. Chem. Chem. Phys, 4, (2002) 198–203.

[65] L. Wu, J. C. Yu and X. Fu, J.Mol. Catal. A: Chem. 244, (2006) 25–32.

[66] A. L. Linsebigler, G. Lu, and J. T. Yates Jr., Chem. Rev. 95, (1995) 735,

[67] M. R. Hofmann, S. T. Martin, W. Choi, and D. W. Bahnemann, Chem. Rev. 95, (1995) 69.

[68] R. Asahi, T. Morikawa, T. Ohwaki, K. Aoki, and Y. Taga, Science. 293, (2001) 269.

[69] M. Gratzel, Nature. 414, (2001) 338.

[70] U. Diebold, Surf. Sci. Rep. 48, (2003) 53-59.

[71] H. Tributsch, Coord. Chem. Rev.248, (2004) 1511-1523.

[72] C. D. Valentin, G. Pacchioni, and A. Selloni, Phys. Rev. B, 70, (2004) 085116-085125.

[73] R. Nakamura, T. Tanaka, and Y. Nakato, J. Phys. Chem. B. 108, (2004) 10617-10621.

[74] M. Miyauchi, A. Ikezawa, H. Tobimatsu, H. Irie, and K. Hashimoto. Chem. Phys. 6, (2004) 865-871.

[75] H. Wang and J. P. Lewis, J. Phys.: Condens. Matter. 18, (2006) 421-426.

[76] S. E. Park, H. Joo, and J. W. Kang, Sol. Energy Mater. Sol. Cells. 83, (2004) 39-45.

[77] S. Karvinen, P. Hirva, and T. A. Pakkanen, Journal of Molecular Structure. 626, (2003) 271-278.

[78] K. Wilke and H. D. Breuer, J. Photochem. Photobiol. A. 121, (1999) 49-54.

[79] C. N. R. Rao. Mater. Sci. Eng., B. 18, (1993)1-6.

[80] E. Santacesaria, M. Tonello, G. Storti, R. C. Pace, and S. Carra, J. Colloid Interface Sci. 111, (1986) 44-49.

[81] Y. Kera, H. Kominami, S. Murakami, and B. Ohtani. Photocatalysis: Science and Technology. Eds. New York: Springer, 2002.

[82] C. Natarajan and G. Nogami, J. Electrochem. Soc. 143, (1996) 1547-1551.

[83] N. R. de Tacconi, C. R. Chenthamarakshan, G. Yogeeswaran, A. Watcharenwong, R. S. de Zoysa, N. A. Basit, and K. Rajeshwar, J. Phys. Chem. B. 110, (2006) 25347.

[84] M. Takeuchi, H. Yamashita, M. Matsuoka, M. Anpo, T. Hirao, N. Itoh, and N. Iwamoto, Catal. Lett. 66, (2000) 185-187.

[85] C. D. Tewillinger and Y. M. Chiang, Nanostruct. Mater. 2(1993) 37-41.

[86] M. K. Akhtar, S. E. Pratsinis, and S. V. R. Mastrangelo, J. Am. Ceram. Soc. 75(1992) 3408-3413.

[87] J. Rubio, J. L. Oteo, M. Villegas, and P. J. Duran, Mater. Sci. 32(1997).

[88] S. J. Kim, D. Hwang, N. Lee, S. Shin, and S. J. Kim, Jpn. J. Appl. Phys., Part 1, 44, (2005) 7703.

[89] M. Schneider and A. Baiker, J. Mater. Chem. 2(1992) 587-593.

[90] P. Billik and G. Plesch, Mater. Lett. 61, (2007)1183-1187.

[91] T. Masui, K. Fujiwara, K. Machida, and G. Adachi, Chem. Mater.,10(1997) 2197.

[92] E. Stathatos, P. Lianos, F. D. Monte, D. Levy, and D. Tsiourvas, Langmuir. 13, (1997) 4296-4300.

[93] Y. V. Kolenko, B. R. Churagulov, M. Kunst, L. Mazerolles, and C. Colbeau-Justin, Appl. Catal., B. 54(2004) 51-57.

[94] K. C. Patil and S. T. Aruna, Redox Methods in SHS Practice, A. A. Borisov, L. DeLuca, and A. Merzhanov, Eds. New York: Taylor and Francis. 2002.

[95] C. M. Wang, H. Wu, and S. L. Chung, J. Poruous Mater., 13(2006) 307.

[96] S. Yamabi and H. Imai, Thin Solid Films, 434(2003) 86.

[97] A. A. Borisov, L. DeLuca, and A. Merzhanov, Eds., Self-Propagating High-Temperature Synthesis of Materials. New York: Taylor and Francis, 2002.

[98] A. Varma, Sci. Amer., 283(2000) 44.

[99] Peter, L. M.; Riley, D. J.; Tull, E. J.; Wijayantha, K. G. Chem.Commun. (2002) 1030−1031.

[100] L. J. Diguna, Q. Shen, J. Kobayashi, T. Toyoda, Appl. Phys.Lett, 91(2007) 023116.

[101] Y. Bessekhouad, D. Robert, Weber, J. V. J. Photochem.Photobiol. A. 163, (2004) 569−580.

[102] M. Nanu, J. Schoonman, A. Goossens, Adv. Funct. Mater. 15, (2005) 95−100.

[103] W. Zhu, X. Liu, H. Q. Liu, D. L. Tong, J. Y. Yang, J. Y. Peng, J. Am. Chem. Soc., 132, (2010) 12619−12626.

[104] R. S. Dibbell and D. F. Watson, J. Phys. Chem. C. 113, (2009) 3139–3149.

[105] R.M.Navarro,F.ValleandJ.L.G.Fierro, Int. J. Hydrogen Energ. 33, (2008) 4265.

[106] C. L. Li, J. Yuan, B. Y. Han, L. Jiang and W. F. Shangguan, Int. J. Hydrogen Energ., 35, (2010) 7073-7077.

[107] H. McDaniel and M. Shim, ACS Nano, 3(2009) 434.

[108] F.Zhang, Y.H. Deng, Y.F. Shi, R.Y. Zhang and D.Y. Zhao, J. Mater.Chem. 20, (2010) 3895-3991.

[109] M. Nyk, R. Kumar, T. Y. Ohulchanskyy, E. J. Bergey and P. N. Prasad,Nano Lett. 8, (2008) 3834.

[110] F. Zhang, G. B. Braun, Y. F. Shi, Y. C. Zhang, X. H. Sun, N. O. Reich,D. Y. Zhao and G. Stucky, J. Am. Chem. Soc., 132(2010) 2850.

[111] B. M. E. Russbueldta and W. F. Hoelderich, J. Catal., (2010) 271,290.

[112] N.Perkas, G. Amirian, Z.Y. Zhong, J. Teo, Y. Gofer and A. Gedanken, Catal. Lett., 130(2009) 455.

[113] P. V. Jyothy, K. A. Amrutha, Jose Gijo and N. V. Unnikrishnan,J. Fluoresc., 19(2009) 165.

[114] J. A. Da ´vila-Pintle,R.Lozada-Morales,M.R.Palomino-MerinoandJ.A.Rivera-Marquez, J. Appl. Phys, 101(2007) 013712.

[115] K. Zhang, D.W. Jing, Q. Y. Chen and L. J. Guo, Int. J. Hydrogen Energy. 35, (2010) 2048.

[116] A. Corma, P. Atienzar, H. Garcia and J. Y. Chane-Ching, Nat. Mater, 3(2004)394.

[117] M. Lira-Cantua and F. C. Krebs, Sol. Energy Mater. Sol. Cells, 90(2006)2076.

[118] H. Kadowaki, N. Saito, H. Nishiyama and Y. Inoue, Chem. Lett.,36(2007) 440.

[119] R. Bamwenda, K. Sayama and H. Arakawa, Chem. Lett.,1047(1999)

[120]Y. S. Chaudhary, S. Panigrahi, S. Nayak, B. Satpati, S. Bhattacharjee andN. Kulkarni, J. Mater. Chem., 20(2010) 2381.

[121] W. I. F. David, K. Shankland, L. B. Mc Cusker and C. Baerlocher, Structure Determination from Powder Diffraction Data, Oxford Science Publications, 1992.

[122] D. L. Bish, J. E. Post and J. E. Modern, Powder Diffraction published by The Mineralogical Society of America, 1989.

[123] L. V. Azaroff and M. J. Buerger, The Powder Method in X-ray Crystallography, McGraw Hill Book Company, Inc, 1975.

[124] M. J. Buerger, X-ray Crystallography, J. Wiley, New York, 20(1942).

[125] L. Smart and E. A. Moore, Solid State Chemistry: an introduction, CRC Press: United States of America, 2005.

[126] S. Brunauer, P. H. Emmet and E. Teller, J. Am. Chem. Soc., 60(1938) 309.

[127] D. B. Williams and C. B. Carter, Transmission Electron Microscopy, Springer,1 (1996).

[128] B. Naik, K. M. Parida, C. S. Gopinath, J. Phys. Chem. C. 114 (2010) 19473-19482.

[129] E. A. Clesceri, A. Greenberg, Standard Methods For Examinations of Water and Wastewater, 19th edn, APHA, AWWA and WEF, Washington, DC, 1995.

[130] N. M. Stover, J. Am. Chem. Soc. 50 (1928) 2363-2366.

[131] Z.Y. Pu, J.Q. Lu, M.F. Luo, Y.L. Xie, Journal of Physical Chemistry C 111 (2007) 18695.

[132] H. Bao, X. Chen, J. Fang, Z. Jiang, W. Huang, Catalysis Letters 125 (2008) 160.

[133] S. Tsunekawa, R. Sivamohan, S. Ito, A. Kasuya, and T. Fukuda, Nanostruct. Mater., 11(1999) 141.

[134] Zhai, T., Fang, X., Bando, Y., Liao, Q., Xu, X., Zeng, H., Ma, Y., Yao, J., Golberg, D., 2009. Morphology-Dependent Stimulated Emission and Field Emission of Ordered CdS Nanostructure Arrays. ACS Nano. 3(949-959).

[135] Xiong, S., Zhang, X., Qian, Y., 2009. CdS with Various Novel Hierarchical Nanostructures by Nanobelts/Nanowires Self-Assembly: Controllable Preparation and Their Optical Properties. Cryst. Growth. Des. 9(5259-5265).

[136] Katari, J. E. B., Colvin, V. L., Alivisatos, A. P., 1994. X-ray Photoelectron Spectroscopy of CdSe Nanocrystals with Applications to Studies of the Nanocrystal Surface. J. Phys. Chem. 98 (4109-4117).

[137] Wang, D., Li, D., Guo, L., Fu, F., Zhang, Z., Wei, Q., 2009. Template-Free Hydrothermal Synthesis of Novel Three-Dimensional Dendritic CdS Nanoarchitectures. J. Phys. Chem. C. 113(5984-5990).

[138] D. R.Mullins, S. H. Overbury and D. R. Huntley, Surf. Sci.,409(1997) 307.

[139] E. Paparazzo, G. M. Ingo and N. Zachetti, J. Vac. Sci. Technol.9(1991) 1416.

[140] G. M. Ingo, R. DalMaschio and L. Scoppio, Surf. Interface Anal.,18(1992), 661.

[141] P. Burroughs, A. Hamnett, A. F. Orchard and G. Thornton,J. Chem. Soc., Dalton Trans., 17(1976) 1686.

[142] S. Sakthivel, H. Kwasch, Daylight Photocatalysis by Carbon-Modified Titanium Dioxide, Angew. Chem. Int. Ed. 42, (2003) 4908-4911.

[143] Ohno, Teruhisa, Tsubota, Toshiki, Toyofukum,Maki, Inaba, Ryoji, Photocatalytic Activity of a TiO2 Photocatalyst Doped with C4+ and S4+ Ions Having a Rutile Phase Under Visible Light, Catal. Lett. 98, (2004) 255-258.

[144] Li, Yuanzhi, Hwang, Doo-Sun, Lee, Nam Hee, Kim, Sun-Jae, Synthesis and characterization of carbon-doped titania as an artificial solar light sensitive photocatalyst, Chem. Phys. Lett. 404 (2005) 25-29.

[145] W. J. Ren, Z. H. Ai, F. L. Jia, L. Z. Zhang, X. X. Fan, Z. G. Zou, Low temperature preparation and visible light photo catalytic activity of mesoporous carbon-doped crystalline TiO2, Appl. Catal. B-Environ. 69 (2007) 138-144.

[146] Tseng, Yao-Hsuan, Kuo, Chien-Sheng, Huang, Chia-Hung, Li, Yuan-Yao, Chou, Po-Wen, Cheng, Chia-Liang, Wong, Ming-Show, Visible-light-responsive nano-TiO_2 with mixed crystal lattice and its photocatalytic activity, Nanotechnology. 17, (2006) 2490-2497.

[147] J.F. Moulder, W.F. Stickle, P.E. Sobol, K.D. Bomben, J. Chastain, Handbook of X-ray Electron Spectroscopy. Perkin-Elmer Corp, Eden Prairie, MN.

[148] N.D. Shinn, K.L. Tsang, Raman Effect in Cadmium Sulfide. J. Vac. Sci. Technol. A. 9, (1992) 1558-1562.

[149] F.-T. Li, Y. Zhao, Y. Liu, Y.-J. Hao, R.-H. Liu and D.-S. Zhao. Chem. Eng. J. 173, (2011) 750–759.

[150] S. Bekkouche, M. Bouhelassa, N.H. Salah, F.Z. Meghlaoui. Desalination. 166, (2004) 355–362.